EBioMedicine 2 (2015) 1034–1047

Contents lists available at ScienceDirect

EBioMedicine

journal homepage: www.ebiomedicine.com

Research Paper

Muscleblind-Like 1 and Muscleblind-Like 3 Depletion Synergistically Enhances Myotonia by Altering *Clc-1* RNA Translation

Jongkyu Choi [a,1], Kirkwood E. Personius [b,1], Marino DiFranco [c,1], Warunee Dansithong [a,2], Carl Yu [c], Saumya Srivastava [a,3], Donald M. Dixon [a], Darshan B. Bhatt [b], Lucio Comai [d], Julio L. Vergara [c], Sita Reddy [a,*]

[a] Department of Biochemistry and Molecular Biology, University of Southern California, Los Angeles, CA 90033, USA
[b] Department of Rehabilitation Science and Program in Neuroscience, School of Public Health and Health Professions, University at Buffalo, Buffalo, NY 14214, USA
[c] Department of Physiology, David Geffen School of Medicine, UCLA, Los Angeles, CA 90095, USA
[d] Department of Microbiology and Immunology, University of Southern California, Los Angeles, CA 90033, USA

ARTICLE INFO

Article history:
Received 25 November 2014
Received in revised form 21 July 2015
Accepted 21 July 2015
Available online 31 July 2015

Keywords:
Muscleblind-like 1
Muscleblind-like 2
Myotonia
Clc-1
RNA translation

ABSTRACT

Loss of Muscleblind-like 1 (Mbnl1) is known to alter *Clc-1* splicing to result in myotonia. $Mbnl1^{\Delta E3/\Delta E3}/Mbnl3^{\Delta E2}$ mice, depleted of Mbnl1 and Mbnl3, demonstrate a profound enhancement of myotonia and an increase in the number of muscle fibers with very low Clc-1 currents, where gCl_{max} values approach ~1 mS/cm^2, with the absence of a further enhancement in *Clc-1* splice errors, alterations in polyA site selection or *Clc-1* localization. Significantly, $Mbnl1^{\Delta E3/\Delta E3}/Mbnl3^{\Delta E2}$ muscles demonstrate an aberrant accumulation of *Clc-1* RNA on monosomes and on the first polysomes. Mbnl1 and Mbnl3 bind *Clc-1* RNA and both proteins bind Hsp70 and eEF1A, with these associations being reduced in the presence of RNA. Thus binding of Mbnl1 and Mbnl3 to *Clc-1* mRNA engaged with ribosomes can facilitate an increase in the local concentration of Hsp70 and eEF1A to assist *Clc-1* translation. Dual depletion of Mbnl1 and Mbnl3 therefore initiates both *Clc-1* splice errors and translation defects to synergistically enhance myotonia. As the HSA^{LR} model for myotonic dystrophy (DM1) shows similar *Clc-1* defects, this study demonstrates that both splice errors and translation defects are required for DM1 pathology to manifest.

Research in context: Research in context: Myotonic Dystrophy type 1 (DM1) is a dominant disorder resulting from the expression of expanded CUG repeat RNA, which aberrantly sequesters and inactivates the muscleblind-like (MBNL) family of proteins. In mice, inactivation of Mbnl1 is known to alter Clc-1 splicing to result in myotonia. We demonstrate that concurrent depletion of Mbnl1 and Mbnl3 results in a synergistic enhancement of myotonia, with an increase in muscle fibers showing low chloride currents. The observed synergism results from the aberrant accumulation of Clc-1 mRNA on monosomes and the first polysomes. This translation error reflects the ability of Mbnl1 and Mbnl3 to act as adaptors that recruit Hsp70 and eEF1A to the Clc-1 mRNA engaged with ribosomes, to facilitate translation. Thus our study demonstrates that Clc-1 RNA translation defects work coordinately with Clc-1 splice errors to synergistically enhance myotonia in mice lacking Mbnl1 and Mbnl3.

1. Introduction

Myotonic Dystrophy type 1 (DM1) is an autosomal dominant disorder resulting from the expansion of a non-coding *CTG* repeat sequence located in the 3′ untranslated region of *DMPK* (Brook et al., 1992; Harper, 2009). In DM1, expanded CUG repeat RNAs (*CUGexp*) aberrantly sequester and disable the muscleblind-like (MBNL) family of splice regulators (Fardaei et al., 2002; Dansithong et al., 2005). Significantly, either *CUGexp* expression or the depletion of Mbnl1 in mouse models has been shown to result in *Clc-1* RNA splice defects and myotonia (Mankodi et al., 2002; Kanadia et al., 2003). This and other lines of evidence have lead DM1 to be considered as a spliceopathy (Ranum and Cooper, 2006). Other studies have implicated the muscleblind proteins in RNA transport, protein secretion and polyadenylation (Adereth et al., 2005; Wang et al., 2012; Batra et al., 2014). However the mechanisms whereby the Mbnl proteins mediate these functions and the role of these novel functional aspects of the Mbnl proteins in disease initiation has yet to be fully understood. In this study we show that the coordinate loss of Mbnl1 and Mbnl3 results in a synergistic enhancement of myotonia and a sharp increase in the number

* Corresponding author at: 2250 Alcazar Street, CSA 240, Institute for Genetic Medicine, University of Southern California, Los Angeles, CA 90033, USA.
E-mail address: sitaredd@usc.edu (S. Reddy).
[1] These authors contributed equally to the study.
[2] Current address: Department of Neurology, Clinical Neurosciences Center, University of Utah, Salt Lake City, UT 84132, USA.
[3] Current address: Department of Neurosciences, Beckman Research Institute of the City of Hope, Duarte, CA 91010, USA.

http://dx.doi.org/10.1016/j.ebiom.2015.07.028

of muscle fibers with extremely low chloride currents. We demonstrate that this synergism does not result from an enhancement in *Clc-1* splice errors, alterations in polyA site selection or *Clc-1* localization but rather reflects the aberrant accumulation of *Clc-1* mRNA on monosomes and the first polysomes in muscles lacking Mbnl1 and Mbnl3. The observed *Clc-1* translation errors reflect the ability of Mbnl1 and Mbnl3 to act as adaptors, recruiting Hsp70 and eEF1A, to *Clc-1* mRNA engaged with ribosomes to facilitate translation. These results therefore demonstrate that *Clc-1* RNA translation defects work coordinately with *Clc-1* splice errors to synergistically enhance myotonia in mice lacking Mbnl1 and Mbnl3. As similar defects are observed in the HSA^{LR} DM1 mouse model, where *CUGexp* aggregate and disable the Mbnl proteins, this study shows that both splice errors and translational defects are required for key features of DM1 pathology to fully manifest.

2. Materials & Methods

2.1. Ethics Statement

All experiments were performed in accordance with the institutional guidelines of the University of Southern California, Los Angeles, University at Buffalo, Buffalo New York and the University of California, Los Angeles. The protocols were approved by the Institutional Animal Care and Use Committee at the University of Southern California, Los Angeles (Protocol number: 10347).

2.2. Muscle Physiology

Contractile properties, electromyography and muscle histology were studied using standard procedures (Reddy et al., 1996; Personius and Arbas, 1998; Personius and Sawyer, 2006). Electrophysiological methods were similar to those described previously (DiFranco et al., 2011). Further details for electrophysiology, solutions and data acquisition are provided in Supplementary Information.

2.3. RNA Analysis

RNA isolation, splicing assays and RT-qPCR analysis were carried out primarily as described in Dansithong et al. (2005). Soleus polyribrosomes were prepared according to a previously described protocol (Darnell et al., 2011) with several modifications. *In vitro* RNA binding assays were carried out as previously described (Paul et al., 2006) with some modifications. Detailed protocols are available in Supplementary Information.

2.4. Purification and Mass Spectrometric Analysis of MBNL3 Complexes

HEK293 cell lines expressing Flag-MBNL3 were generated by transfection of a pCDNA3.1-Flag-MBNL3 vector. Experimental details, including purification and mass spectrometric analysis of MBNL3 complexes are provided in Supplementary Information.

2.5. 3′RACE and PCR

For 3′RACE, total RNA was reverse transcribed using 3′RACE System for Rapid Amplification of cDNA Ends kits (Life Technologies, USA) with the adapter primer (AP-3′RACE: 5′-AAG CAG TGG TAA CAA CGC AGA GTA CTT TTT TTT TTT TTT TTT TTT TTT TTT TVN-3′). Target cDNAs were amplified by PCR and nested PCR with gene-specific forward primers and the amplification primer (AP: 5′-AAG CAG TGG TAA CAA CGC AGA GT-3′). The relative band intensities were measured by densitometry analysis using Gene Tool (Syngene Inc., USA). To identify the Poly(A) sites, bands were excised and extracted using gel extraction kit (Qiagne, USA). Extracted DNAs were cloned into pGEM-T Easy Vector (Promega, USA) according to the manufacturer's protocol. The DNA inserts were sequenced using the customized sequencing primers, T7 and SP6 promoter sequencing primers (Integrated DNA Technologies Inc., USA). The gene-specific forward primers and sequencing primers are as listed in Table S1.

3. Results

3.1. Development of $Mbnl2^{GT2/GT2}$ and $Mbnl3^{\Delta E2}$ Mice

We developed 129sv *Mbnl2* gene trap ($Mbnl2^{GT2/GT2}$) mice derived from a BayGenomic ES cell line in which a retroviral β-geo gene trap is integrated downstream of *Mbnl2* exon 2 (Fig. 1A–C). Chimeric animals derived from targeted 129sv ES cells were bred to 129sv wild type animals to derive 129sv $Mbnl2^{+/GT2}$ mice. Analysis of genotype ratios of the progeny of $Mbnl2^{+/GT2}$ crosses did not reveal an $Mbnl2^{GT2/GT2}$ lethal phenotype. In the $Mbnl2^{GT2/GT2}$ mice transcription beyond the polyA site in the β-geo cassette in conjunction with the absence of the utilization of the β-geo splice acceptor site can result in the production of the normal transcript. Therefore we measured Mbnl2 levels using the MB2a monoclonal antibodies (Holt et al., 2009) and observe that Mbnl2 levels were decreased by ~85% in $Mbnl2^{GT2/GT2}$ mice (Fig. 1D).

In parallel experiments we developed male $Mbnl3^{\Delta E2}$ and female $Mbnl3^{\Delta E2/\Delta E2}$ mice in which exon 2 of the X-linked *Mbnl3* gene was replaced by a Neomycin expression cassette (Fig. 1E & F). Exon 2 encodes the translation start site for the full-length 38 kD Mbnl3 protein ($Mbnl3_{38kD}$). Chimeric animals derived from targeted 129sv ES cells were bred to 129sv wild type animals to derive $Mbnl3^{+/\Delta E2}$ mice. Analysis of genotype ratios of the progeny of male $Mbnl3^{\Delta E2}$ and female $Mbnl3^{\Delta E2/\Delta E2}$ mice did not reveal a homozygous mutant lethal phenotype. For simplicity, male and female mice lacking Mbnl3 exon2 are indicated as $Mbnl3^{\Delta E2}$.

Poulos et al. have described a C57BL6 mouse strain in which Mbnl3 exon 2 was deleted (Poulos et al., 2013). These authors identified a 27 kD Mbnl3 isoform ($Mbnl3_{27kD}$), resulting from the use of a second translation start site located in *Mbnl3* exon 3. In their study, deletion of Mbnl3 exon 2 resulted in the loss of the full-length $Mbnl3_{38kD}$ protein and retention of the truncated $Mbnl3_{27kD}$ isoform (Poulos et al., 2013). We developed polyclonal antibodies using an Mbnl3 C-terminal peptide as previously described (Poulos et al., 2013) to characterize Mbnl3 expression in our 129sv $Mbnl3^{\Delta E2}$ mouse strain. Consistent with the results of Poulos et al., we observe loss of the full-length $Mbnl3_{38kD}$ protein and retention of the truncated $Mbnl3_{27kD}$ isoform in $Mbnl3^{\Delta E2}$ placenta, a tissue that expresses high levels of Mbnl3 (Fig. 1G & H). Previous studies have shown elevated levels of *Mbnl3* mRNA in stem cells and in multiple tissues during embryogenesis with diminished expression in adult human and mouse tissues (Fardaei et al., 2002; Poulos et al., 2013). RT-PCR analyses demonstrate detectable *Mbnl3* exon 2 RNA expression in the C57BL6 and the 129sv adult wild type skeletal muscles but not in $Mbnl3^{\Delta E2}$ skeletal muscles (Figs. 1I and S1 & S2).

3.2. $Mbnl2^{GT2/GT2}$ and $Mbnl3^{\Delta E2}$ Skeletal Muscles Do Not Show DM1 Specific Splice Defects

$Mbnl2^{GT2/GT2}$ and $Mbnl3^{\Delta E2}$ lower limb muscles were dissected and the RNA from these tissues was examined for DM1 specific splice defects in a sample set of four RNAs, *Ldb3*, *Clc-1*, *mTitin* and *Atp2a1* (Lin et al., 2006). In these experiments no significant change in the splicing of these RNAs in $Mbnl2^{GT2/GT2}$ and $Mbnl3^{\Delta E2}$ skeletal muscles was observed when compared with wild type controls (Fig. S3). In parallel experiments no overt changes in muscle structure or function were detected.

3.3. $Mbnl1^{\Delta E3/\Delta E3}$/$Mbnl2^{GT2/GT2}$ Mice Demonstrate a Lethal Phenotype

To test the combinatorial effects of dose reductions in Mbnl1 and Mbnl2 we examined the genotypes of the progeny from an $Mbnl1^{+/\Delta E3}$ X $Mbnl2^{+/GT2}$ cross. $Mbnl1^{+/\Delta E3}$ mice, in which a Neomycin cassette replaces *Mbnl1* exon 3, are a gift of Dr. Swanson and have been previously

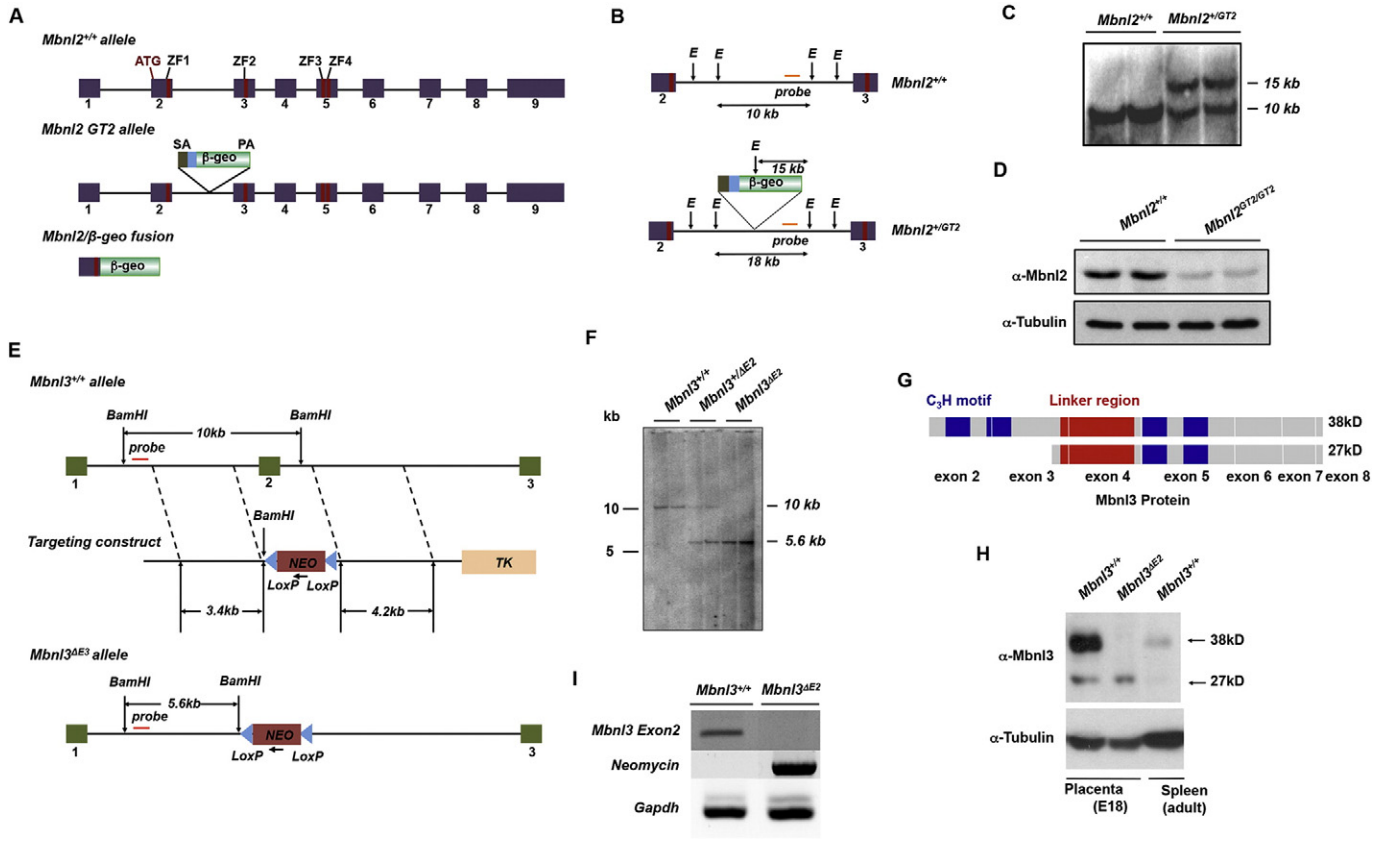

Fig. 1. Development of *Mbnl2*$^{GT2/GT2}$ and *Mbnl3*$^{\Delta E2}$ mice. (A) *Mbnl2* wild type allele, *Mbnl2*^{GT2} allele and the Mbnl2 β-geo fusion protein are shown. SA: splice acceptor; and PA: Poly A sequence. ZnF motifs are shown as red boxes. (B–C) Southern blot analysis of tail clip DNA from wild type (*Mbnl2*$^{+/+}$) and *Mbnl2*$^{+/GT2}$ mice restricted with EcoRI and hybridized to the probe indicated in orange (B) is shown. (D) Skeletal muscle protein extracts from wild type (*Mbnl2*$^{+/+}$) and *Mbnl2*$^{GT2/GT2}$ mice examined for Mbnl2 expression using the MB2a antibodies by Western blot analysis. Tubulin was used as an internal control. (E) *Mbnl3* wild type allele, the targeting vector and the *Mbnl3*$^{\Delta E2}$ allele is shown. (F) Southern blot analysis of tail clip DNA from wild type (*Mbnl3*$^{+/+}$), *Mbnl3*$^{+/\Delta E2}$ and *Mbnl3*$^{\Delta E2}$ mice restricted with BamHI and hybridized to the probe indicated in red (E). (G) Structure of the Mbnl3$_{38kD}$ and Mbnl3$_{27kD}$ isoforms. Tandem ZnF motifs (C_3H motif, blue boxes) and the linker region (red box) are indicated. (H) Western blot analysis of Mbnl3 expression. *Mbnl3*$^{+/+}$ and *Mbnl3*$^{\Delta E2}$ E18 placenta and adult *Mbnl3*$^{+/+}$ spleen protein extracts were examined for Mbnl3 expression using C-terminal peptide derived anti-Mbnl3 antibodies by Western blot analysis. Tubulin was used as an internal control. (I) RT-PCR analysis of wild type and *Mbnl3*$^{\Delta E2}$ skeletal muscle RNA using primers located in *Mbnl3* exon 2 and in the Neomycin gene. *Gapdh* was amplified in parallel as a loading control.

described by Kanadia et al., (2003). These animals were backcrossed onto a 129sv background for 4 generations prior to use in our experiments. *Mbnl2*$^{GT2/GT2}$/*Mbnl1*$^{\Delta E3/\Delta E3}$ animals were not observed in the ~300 progeny examined, consistent with the lethality of the *Mbnl1*$^{\Delta E3/\Delta E3}$/*Mbnl2*$^{GT2/GT2}$ genotype.

3.4. *Mbnl1*$^{\Delta E3/\Delta E3}$/*Mbnl3*$^{\Delta E2}$ Mice Show Enhanced Myotonic Activity

In contrast to the lethal phenotype observed in the *Mbnl2*$^{GT2/GT2}$/*Mbnl1*$^{\Delta E3/\Delta E3}$ animals, dual loss of Mbnl1 and Mbnl3 results in viable *Mbnl1*$^{\Delta E3/\Delta E3}$/*Mbnl3*$^{\Delta E2}$ animals that demonstrate a synergistic enhancement of skeletal muscle myotonia. As reported previously for the vastus muscle, runs of myotonic activity were observed in both the EDL and soleus muscles following needle insertion in *Mbnl1*$^{\Delta E3/\Delta E3}$ mice with myotonic activity averaging at 3.07 ± 1.46 s in the EDL and 3.98 ± 2.10 s in the soleus (mean ± SEM, Tables 1 & 2) (Kanadia et al., 2003). In striking contrast, the length of myotonic activity was four to ten folds greater in *Mbnl1*$^{\Delta E3/\Delta E3}$/*Mbnl3*$^{\Delta E2}$ mice with average run lengths of 17.1 ± 3.88 s in the EDL and 32.3 ± 26.7 s in the soleus (mean ± SEM, Tables 1 & 2). The longest run of myotonic activity detected from *Mbnl1*$^{\Delta E3/\Delta E3}$ and *Mbnl1*$^{\Delta E3/\Delta E3}$/*Mbnl3*$^{\Delta E2}$ mice is shown in Fig. 2A & B. The runs show the characteristic waxing/waning amplitude and frequency of myotonic electrical activity with the longest run lengths being 8.1 s and 26 s for *Mbnl1*$^{\Delta E3/\Delta E3}$ and *Mbnl1*$^{\Delta E3/\Delta E3}$/*Mbnl3*$^{\Delta E2}$ mice, respectively.

Duration of post-insertional EMG activity was significantly increased only in *Mbnl1*$^{\Delta E3/\Delta E3}$ and *Mbnl1*$^{\Delta E3/\Delta E3}$/*Mbnl3*$^{\Delta E2}$ mice when compared to wild type controls (ANOVA on ranks with Dunn's post-hoc analysis, $p < 0.001$) (Fig. 2C). Heterozygous deletion of *Mbnl1* does not appear to be sufficient to produce myotonic activity in the EDL or soleus muscles, since average post-insertional EMG activity averaged only 0.20 ± 0.03 s in the EDL and 0.26 ± 0.05 s in the soleus. These values are similar to those found in wild type mice (0.17 ± 0.02 s in the EDL and 0.19 ± 0.03 s in the soleus, Tables 1 & 2). Only *Mbnl1*$^{\Delta E3/\Delta E3}$ and *Mbnl1*$^{\Delta E3/\Delta E3}$/*Mbnl3*$^{\Delta E2}$ mice demonstrate spontaneous myofiber electrical activity. Spontaneous spiking was found in 50% of *Mbnl1*$^{\Delta E3/\Delta E3}$ and 75% of *Mbnl1*$^{\Delta E3/\Delta E3}$/*Mbnl3*$^{\Delta E2}$ muscles.

Table 1
Soleus muscle weight and EMG run length.

Genotype	Muscle wgt (mg)	EMG run length (s)	n
Wild type	6.31 ± 0.45	0.19 ± 0.03	9
Mbnl1$^{\Delta E3/\Delta E3}$	7.78 ± 1.14	3.98 ± 2.10	8
Mbnl2$^{GT2/GT2}$	7.17 ± 0.60	0.13 ± 0.01	5
Mbnl3$^{\Delta E2}$	7.57 ± 0.20	0.19 ± 0.03	6
Mbnl1$^{\Delta E3/\Delta E3}$/*Mbnl3*$^{\Delta E2}$	5.80 ± 0.49	32.3 ± 26.7	4
Mbnl2$^{GT2/GT2}$/*Mbnl3*$^{\Delta E2}$	5.86 ± 0.55	0.26 ± 0.03	7
Mbnl1$^{+/\Delta E3}$/*Mbnl2*$^{GT2/GT2}$	8.25 ± 0.95	0.26 ± 0.05	3
p-Value	*0.254	**# < 0.001**	

(*) One-way ANOVA and Student *t*-tests with Bonferroni correction were used to determine paired differences between *Mbnl* genotype and wild type mice. (#) ANOVA on ranks with Dunn's post-hoc analysis was used for data with non-normal distribution. Bold indicates the statistically significant ($p < 0.05$).

Table 2
EDL contractile properties and EMG run length.

Genotype	Animal wgt (9)	Muscle wgt (mg)	sPo (N/cm^2)	Pt (N/cm^2)	% Fatigue (3 min)	EMG run length (s)	n
Wild type	34.9 ± 2.5	9.07 ± 0.32	21.4 ± 1.5	3.89 ± 0.24	82.2 ± 3.4	0.17 ± 0.02	15
Mbnl1$^{\Delta E3/\Delta E3}$	28.8 ± 2.1	9.78 ± 0.91	15.1 ± 2.9	2.87 ± 0.55	82.7 ± 6.1	3.07 ± 1.46	8
Mbnl2$^{GT2/GT2}$	33.7 ± 1.4	8.50 ± 0.34	19.8 ± 2.1	4.30 ± 0.56	82.3 ± 1.9	0.22 ± 0.02	6
Mbnl3$^{\Delta E2}$	39.3 ± 4.0	9.43 ± 0.20	25.7 ± 3.0	4.63 ± 0.44	82.1 ± 2.6	0.22 ± 0.03	7
Mbnl1$^{\Delta E3/\Delta E3}$/*Mbnl3*$^{\Delta E2}$	27.9 ± 1.6	10.08 ± 1.32	13.1 ± 2.1	2.75 ± 0.42	85.3 ± 1.0	17.1 ± 3.88	5
Mbnl2$^{T2GT2/GT2}$/*Mbnl3*$^{\Delta E2}$	30.4 ± 2.7	7.25 ± 0.25	20.2 ± 2.2	4.25 ± 0.55	85.3 ± 1.3	0.30 ± 0.03	6
Mbnl1$^{+/\Delta E3}$/*Mbnl2*$^{GT2/GT2}$	37.4 ± 4.5	9.75 ± 0.63	16.9 ± 3.1	2.96 ± 0.50	79.8 ± 4.3	0.20 ± 0.03	4
p-Value	*0.082	*0.072	***0.018**	***0.027**	*0.704	**# < 0.001**	

sPo: Specific maximal muscle force production and Pt: specific twitch force production.
% Fatigue: The percent decrease in force production over 3 min.
(*) One-way ANOVA and Student *t*-tests with Bonferroni correction were used to determine paired differences between *Mbnl* genotypes and wild type mice. (#) ANOVA on ranks with Dunn's post-hoc analysis was used for data with non-normal distribution. Bold indicates the statistically significant ($p < 0.05$).

3.5. *Mbnl1*$^{\Delta E3/\Delta E3}$/*Mbnl3*$^{\Delta E2}$ Mice Show Diminished Force Production

To test the effect of Mbnl dose reductions on specific force we measured maximal isometric specific force produced by the EDL muscle in wild type, *Mbnl1*$^{\Delta E3/\Delta E3}$, *Mbnl2*$^{GT2/GT2}$, *Mbnl3*$^{\Delta E2}$, *Mbnl1*$^{\Delta E3/\Delta E3}$/*Mbnl3*$^{\Delta E2}$, *Mbnl2*$^{GT2/GT2}$/*Mbnl3*$^{\Delta E2}$ and *Mbnl1*$^{+/\Delta E3}$/*Mbnl2*$^{GT2/GT2}$ mice. In these experiments, animal weight and EDL muscle weight were similar across all experimental groups (Table 2). Reduced force generation per cross sectional area (CSA) is only seen in *Mbnl1*$^{\Delta E3/\Delta E3}$ and *Mbnl1*$^{\Delta E3/\Delta E3}$/*Mbnl3*$^{\Delta E2}$ mice when compared to wild type controls (one-way ANOVA, $p = 0.018$), with *Mbnl1*$^{\Delta E3/\Delta E3}$ mice showing an intermediate reduction in force and *Mbnl1*$^{\Delta E3/\Delta E3}$/*Mbnl3*$^{\Delta E2}$ mice showing a further diminishment of specific force (Specific force decreased 29.4% and 38.8% compared to wild type mice for *Mbnl1*$^{\Delta E3/\Delta E3}$ and *Mbnl1*$^{\Delta E3/\Delta E3}$/*Mbnl3*$^{\Delta E2}$ mice, respectively) (Fig. 2D). *Mbnl1*$^{+/\Delta E3}$/*Mbnl2*$^{GT2/GT2}$ mice demonstrate mild weakness, suggesting that complete loss of Mbnl1 is necessary to result in significant loss of muscle force production.

Reduced force production in both *Mbnl1*$^{\Delta E3/\Delta E3}$ and *Mbnl1*$^{\Delta E3/\Delta E3}$/*Mbnl3*$^{\Delta E2}$ mice was seen at stimulation frequencies between 65–200 Hz. The similar shapes of the force-frequency curves (Fig. 2E) demonstrate that depletion of Mbnl1 or Mbnl1 and Mbnl3 do not affect the stimulation frequency necessary to produce maximal force production. These data suggest limited changes in the distribution of muscle fiber-types between *Mbnl1*$^{\Delta E3/\Delta E3}$ and *Mbnl1*$^{\Delta E3/\Delta E3}$/*Mbnl3*$^{\Delta E2}$ mice. As seen for maximal specific force, muscle force produced following a single 0.2 ms stimulation (twitch force, Pt) was reduced only in *Mbnl1*$^{\Delta E3/\Delta E3}$, *Mbnl1*$^{\Delta E3/\Delta E3}$/*Mbnl3*$^{\Delta E2}$ and *Mbnl1*$^{+/\Delta E3}$/*Mbnl2*$^{GT2/GT2}$ mice (one-way ANOVA, $p = 0.027$) (Table 2). Consistent with maximal specific force measurements, twitch force was modestly decreased in *Mbnl1*$^{+/\Delta E3}$/*Mbnl2*$^{GT2/GT2}$ animals, with intermediate and maximal reduction in this series being observed in *Mbnl1*$^{\Delta E3/\Delta E3}$ and *Mbnl1*$^{\Delta E3/\Delta E3}$/*Mbnl3*$^{\Delta E2}$ mice, respectively (Pt decreased 26.2% and 29.3% compared to wild type mice for *Mbnl1*$^{\Delta E3/\Delta E3}$ and *Mbnl1*$^{\Delta E3/\Delta E3}$/*Mbnl3*$^{\Delta E2}$ mice, respectively). Finally, no differences in the extent of muscle fatigue following 3 min of contraction at a 1/3 duty cycle was seen between genotypes further supporting limited changes in the distribution of muscle fiber-types in these genotypes (Table 2).

3.6. *Mbnl1*$^{\Delta E3/\Delta E3}$/*Mbnl3*$^{\Delta E2}$ Muscles Demonstrate Centralized Nuclei, Atrophic Fibers and Regions of Potential Fibrosis

EDL muscle sections from wild type, *Mbnl1*$^{\Delta E3/\Delta E3}$, *Mbnl2*$^{GT2/GT2}$, *Mbnl3*$^{\Delta E2}$ and *Mbnl1*$^{\Delta E3/\Delta E3}$/*Mbnl3*$^{\Delta E2}$ mice were examined for myopathic changes subsequent to H&E stains ($n = 3$ mice per genotype). *Mbnl2*$^{GT2/GT2}$ and *Mbnl3*$^{\Delta E2}$ mice show no histopathological changes. As previously reported *Mbnl1*$^{\Delta E3/\Delta E3}$ mice demonstrate mild myopathy with regions of muscle fibers containing centralized nuclei (Kanadia et al., 2003). In contrast, muscle sections from *Mbnl1*$^{\Delta E3/\Delta E3}$/*Mbnl3*$^{\Delta E2}$ mice demonstrate some centralized nuclei, areas of very small atrophied fibers and regions of potential fibrosis (Fig. 2F). Average muscle fiber perimeter was 127 ± 3, 113 ± 7, 111 ± 15, 128 ± 40, and 138 ± 9 μm for wild type, *Mbnl1*$^{\Delta E3/\Delta E3}$, *Mbnl1*$^{\Delta E3/\Delta E3}$/*Mbnl3*$^{\Delta E2}$, *Mbnl2*$^{GT2/GT2}$ and *Mbnl3*$^{\Delta E2}$ mice, respectively. No difference was seen between any Mbnl deficient genotypes and wild type mice, however a trend towards muscle fiber CSA reduction was observed in *Mbnl1*$^{\Delta E3/\Delta E3}$ and *Mbnl1*$^{\Delta E3/\Delta E3}$/*Mbnl3*$^{\Delta E2}$ mice, with an opposing trend of an increase in muscle fiber CSA observed in *Mbnl2*$^{GT2/GT2}$ and *Mbnl3*$^{\Delta E2}$ mice (Frequency histograms of muscle fiber CSA and perimeter are shown in Fig. S4).

3.7. Clc-1 Immunohistochemistry in *Mbnl1*$^{\Delta E3/\Delta E3}$/*Mbnl3*$^{\Delta E2}$ and *Mbnl1*$^{\Delta E3/\Delta E3}$ Muscles

To decipher the mechanism underlying the enhanced myotonia observed in *Mbnl1*$^{\Delta E3/\Delta E3}$/*Mbnl3*$^{\Delta E2}$ mice Clc-1 protein expression was examined by semi-quantitative immunoflourescence studies. Immunoflourescence analyses were utilized, as commercially available anti-Clc-1 antibodies are unable to detect chloride channels by Western blot analyses. Clc-1 protein expression was identified by immunofluorescence using antibodies against the C terminus (CLC1 1-A; Alpha Diagnostic) and imaged by confocal microscopy. Since the intensity of Clc-1 immunofluorescence was relatively low, the confocal pin-hole was opened to 1.12 airy units to improve image brightness. Images were not deconvolved to better identify receptor localization (Fig. 2G). The images observed using this protocol closely resemble confocal images of Ca_v 1.1 and Ca_v 1.2 Ca^{2+} expression in skeletal muscle (Jeftinija et al., 2007). As a first attempt to quantify Clc-1 expression, we measured Clc-1 immunofluorescence in 15 membrane regions for each confocal image (80 μm^2 ovals). The grayscale intensity of Clc-1 membrane immunolabeling was decreased in *Mbnl3*$^{\Delta E2}$ and *Mbnl1*-$^{\Delta E3/\Delta E3}$/*Mbnl3*$^{\Delta E2}$ muscles compared to wild type, *Mbnl2*$^{GT2/GT2}$ and *Mbnl3*$^{\Delta E2}$ muscles ($p < 0.001$). Specifically, average gray scale values were 36 ± 3, 24 ± 1, 20 ± 1, 38 ± 3, and 39 ± 4 GSE for wild type, *Mbnl1*$^{\Delta E3/\Delta E3}$, *Mbnl1*$^{\Delta E3/\Delta E3}$/*Mbnl3*$^{\Delta E2}$, *Mbnl2*$^{GT2/GT2}$ and *Mbnl3*$^{\Delta E2}$ mice, respectively. Thus Clc-1 protein expression appeared to be consistently reduced in *Mbnl1*$^{\Delta E3/\Delta E3}$ and *Mbnl1*$^{\Delta E3/\Delta E3}$/*Mbnl3*$^{\Delta E2}$ mice when compared to wild type, *Mbnl2*$^{GT2/GT2}$, and *Mbnl3*$^{\Delta E2}$ animals ($n = 3$ mice per genotype, Fig. 2G).

3.8. Chloride Currents Recorded in *Mbnl1*$^{\Delta E3/\Delta E3}$/*Mbnl3*$^{\Delta E2}$ Fibers are Smaller Than Those of *Mbnl1*$^{\Delta E3/\Delta E3}$ and Wild Type Fibers

Examination of chloride currents (ICl) was carried out subsequently to assess potential functional differences between *Mbnl1*$^{\Delta E3/\Delta E3}$, *Mbnl3*$^{\Delta E2}$ and *Mbnl1*$^{\Delta E3/\Delta E3}$/*Mbnl3*$^{\Delta E2}$ mice. Since the total ICl recorded from a single muscle fiber depends on its physical dimensions (length and radius), in these experiments we normalized the raw currents by both the fibers' surface area (μA/cm^2) and capacitance (A/F). As our previous work has shown that a large fraction of ICl arises from the T tubule system (TTS) of adult mice (DiFranco et al., 2011), the latter normalization would take into account the contribution of the TTS to the total membrane area of a fiber. ICl records in response to the 3-pulse protocol obtained

from a wild type (129SV) fiber are shown in Fig. 3A. These currents show the canonical features of ICl that have previously been reported for adult wild type C57BL6 mice (DiFranco et al., 2011). Specifically, immediately following maximal activation during a long depolarization to +60 mV (pre-pulse), ICl records during test pulses show the typical inward rectification pattern with smaller steady outward currents (Fig. 3A, blue, gold, pink, and dark cyan traces) in response to depolarizing pulses, and larger transient inward currents with voltage-dependent deactivation rates (Fig. 3A, red, green, blue, orange and purple traces) in response to hyperpolarizing pulses. In the wild type 129sv fiber, the peak ICl in

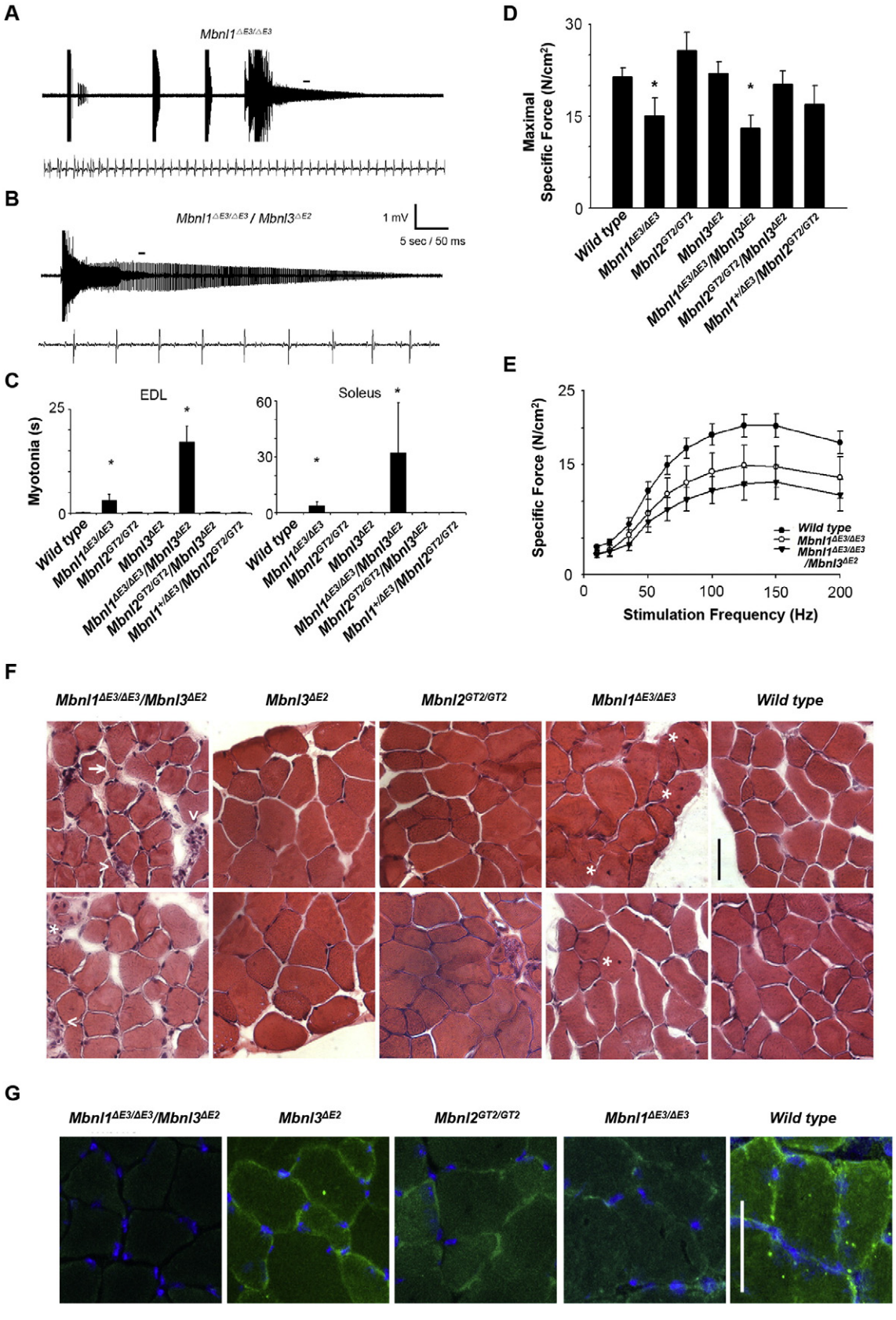

response to a −120 mV pulse ($[peak\ ICl]_{max}$) was −817 μA/cm² (−147 A/F), which is comparable to the −710 ± 58 μA/cm² (137 ± 11 A/F; mean ± SEM), obtained under the same conditions and age, in wild type C57BL6 mice (DiFranco et al., 2011). Consistent with previous results in fibers from immature (9–14 days) *Mbnl1*$^{\Delta E3/\Delta E3}$ mice (Lueck et al., 2007), our ICl records in fibers from adult (3–4 months) *Mbnl1*$^{\Delta E3/\Delta E3}$ mice are generally smaller than those from wild type fibers (Fig. 3A & B). However, for the *Mbnl1*$^{\Delta E3/\Delta E3}$ fiber shown in Fig. 3B the $[peak\ ICl]_{max}$ was −551 μA/cm² (−118 A/F), which represents a reduction of only 33% with respect to the wild type fiber shown in Fig. 3A. Average values for $[peak\ ICl]_{max}$ are −770 ± 34 μA/cm² (−156 ± 8 A/F; n = 16) and −507 ± 28 μA/cm² (−116 ± 7 A/F; n = 19) for fibers from wild type and *Mbnl1*$^{\Delta E3/\Delta E3}$ mice, respectively. From these values, a 34% reduction is calculated.

Unlike ICl from *Mbnl1*$^{\Delta E3/\Delta E3}$ fibers, currents from *Mbnl3*$^{\Delta E2}$ fibers were not altered; the $[peak\ ICl]_{max}$ in *Mbnl3*$^{\Delta E2}$ fibers was −799 ± 26 μA/cm² (−169 ± 6 A/F; n = 37), which is not significantly different ($p > 0.3$) from the average values in wild type mice. Since *Mbnl1*$^{\Delta E3/\Delta E3}$/*Mbnl3*$^{\Delta E2}$ mice display more marked myotonia than *Mbnl1*$^{\Delta E3/\Delta E3}$ animals, we tested if the severity of the myotonia results from further impairments in ICl in *Mbnl1*$^{\Delta E3/\Delta E3}$/*Mbnl3*$^{\Delta E2}$ animals. This would be particularly intriguing since fibers from *Mbnl3*$^{\Delta E2}$ mice have normal ICl. Fig. 3C shows that, while the main features of the ICl records are preserved, the overall magnitudes of the currents are further reduced in fibers from *Mbnl1*$^{\Delta E3/\Delta E3}$/*Mbnl3*$^{\Delta E2}$ mice when compared to those from *Mbnl1*$^{\Delta E3/\Delta E3}$ fibers (Fig. 3B). The $[peak\ ICl]_{max}$ in the *Mbnl1*$^{\Delta E3/\Delta E3}$/*Mbnl3*$^{\Delta E2}$ fiber in Fig. 3C is −412 μA/cm² (−107 A/F), representing ~50% of the current in wild type mice in Fig. 3A. A comparable and significant ($p < 0.05$) reduction was found for the average peak ICl in 16 fibers from *Mbnl1*$^{\Delta E3/\Delta E3}$/*Mbnl3*$^{\Delta E2}$ mice (−410 ± 55 μA/cm², or −90 ± 14 A/F) with respect to those from wild type mice. The additional 13% reduction in peak *Mbnl1*$^{\Delta E3/\Delta E3}$/*Mbnl3*$^{\Delta E2}$ ICl with respect to *Mbnl1*$^{\Delta E3/\Delta E3}$ fibers, is statistically significant ($p < 0.05$).

3.9. Voltage-Dependence of ICl in Wild Type, *Mbnl1*$^{\Delta E3/\Delta E3}$ and *Mbnl1*$^{\Delta E3/\Delta E3}$/*Mbnl3*$^{\Delta E2}$ Fibers

In order to further establish the comparative differences in the functional expression of Clc-1 in *Mbnl* mutant mice, we investigated whether the voltage-dependence of the peak (instantaneous) and steady-state I–V plots of ICl were preserved in wild type, *Mbnl1*$^{\Delta E3/\Delta E3}$, *Mbnl3*$^{\Delta E2}$ and *Mbnl1*$^{\Delta E3/\Delta E3}$/*Mbnl3*$^{\Delta E2}$ animals. Panels D–F in Fig. 3 show that peak ICl plots (black symbols) in all three mouse strains display similar inward rectification properties. Importantly, the magnitudes of the ICl are differentially affected in the *Mbnl1*$^{\Delta E3/\Delta E3}$ and *Mbnl1*$^{\Delta E3/\Delta E3}$/*Mbnl3*$^{\Delta E2}$ mice when compared to wild type mice. Specifically, Fig. 3D reveals almost identical properties for wild type (black closed symbols and solid line) and *Mbnl3*$^{\Delta E2}$ (black open symbols and dashed line) fibers. In contrast, peak data from *Mbnl1*$^{\Delta E3/\Delta E3}$ and *Mbnl1*$^{\Delta E3/\Delta E3}$/*Mbnl3*$^{\Delta E2}$ mice, must be scaled by 1.46 and 1.88 factors (respectively), in order to become superimposable with those from wild type animals (not shown). Likewise, the steady-state ICl plots (red symbols and lines) showing the characteristic inverted bell shape of Clc-1 can be scaled using similar proportions with those of their respective peak ICl in order to match the data from wild type mice. Thus these data demonstrate that the functional expression of Clc-1 is normal in *Mbnl3*$^{\Delta E2}$ mice, but reduced to ~34% and ~47% in *Mbnl1*$^{\Delta E3/\Delta E3}$ and *Mbnl1*$^{\Delta E3/\Delta E3}$/*Mbnl3*$^{\Delta E2}$ mice, respectively ($p < 0.05$). Taken in conjunction with the Clc-1 immunohistochemistry analyses, these data support the model that the intrinsic properties of Clc-1 channels are not altered in *Mbnl1*$^{\Delta E3/\Delta E3}$ and *Mbnl1*$^{\Delta E3/\Delta E3}$/*Mbnl3*$^{\Delta E2}$ mice and that the deficiency in current magnitude is related to a diminished density in channel expression.

3.10. Reduction of Maximal Slope Conductance in *Mbnl1*$^{\Delta E3/\Delta E3}$ and *Mbnl1*$^{\Delta E3/\Delta E3}$/*Mbnl3*$^{\Delta E2}$ Fibers

A more comprehensive way to demonstrate the reduction in the expression of functional Clc-1 channels in *Mbnl* mutant muscles is to evaluate the maximal (limiting) slope conductance (gCl_{max}), as obtained from the instantaneous I–V plots of ICl. Fig. 3G shows that, in correspondence with the data from the previous plots, gCl_{max} is large in wild type (7.0 ± 0.31 mS/cm², or 1.39 ± 0.09 mS/μF; n = 16) and *Mbnl3*$^{\Delta E2}$ (7.4 ± 0.27 mS/cm², or 1.57 ± 0.06 mS/μF; n = 37), minimal in *Mbnl1*$^{\Delta E3/\Delta E3}$/*Mbnl3*$^{\Delta E2}$ (3.5 ± 0.52 mS/cm², or 0.80 ± 0.12 mS/μF; n = 16), and intermediate (4.9 ± 0.29 mS/cm²; 1.12 ± 0.06 mS/μF; n = 18) in *Mbnl1*$^{\Delta E3/\Delta E3}$ mice. In addition, gCl_{max} from fibers of *Mbnl1*$^{\Delta E3/\Delta E3}$/*Mbnl3*$^{\Delta E2}$ mice were significantly smaller than those from *Mbnl1*$^{\Delta E3/\Delta E3}$ mice. The statistical significance between gCl_{max} values was independent of the normalization factor (area or capacitance).

3.11. Frequency Distribution of gCl_{max} in Fibers from Mbnl Mutant Mice

We have shown that myotonia as reported by EMG is more pronounced in *Mbnl1*$^{\Delta E3/\Delta E3}$/*Mbnl3*$^{\Delta E2}$ mice when compared to *Mbnl1*$^{\Delta E3/\Delta E3}$ mice and that the average peak ICl (and $[peak\ ICl]_{max}$) is smaller in the *Mbnl1*$^{\Delta E3/\Delta E3}$/*Mbnl3*$^{\Delta E2}$ muscles when compared with *Mbnl1*$^{\Delta E3/\Delta E3}$ muscles. Nevertheless, the data on the functional expression of Clc-1 channel reported here are incompatible with the classic claim that the genesis of myotonia requires reductions in gCl larger than 70% (Furman and Barchi, 1978). In order to examine this apparent discrepancy, we compared the frequency distribution of gCl_{max} in fibers from the wild type and the *Mbnl* strains (Fig. 4). Each dataset was fitted with a normal distribution (shown with solid lines) and for the purpose of comparison, the normal curve fitted to the data from the wild type mice is shown superimposed to the data from the *Mbnl* mutant strains. It can be observed that the gCl_{max} histograms for fibers of wild type and *Mbnl3*$^{\Delta E2}$ mice (Fig. 4A and B) are very similar to each other, and the medians are centered at almost identical average values. These results are in agreement with both the lack of myotonia and the normal ICl in *Mbnl3*$^{\Delta E2}$ mice. In contrast, when the data obtained from wild type and *Mbnl1*$^{\Delta E3/\Delta E3}$ mice are compared (Fig. 4C), the average gCl_{max} is clearly shifted to the left, and that there are a significant number of fibers with very small gCl_{max} values that are outside the normal distribution of wild type animals. We propose that, although on-average gCl_{max} is not drastically reduced in *Mbnl1*$^{\Delta E3/\Delta E3}$ mice, the small but significant numbers of severely affected fibers may explain the mild myotonia in these animals. This explanation is consistent with the observation that the *Mbnl1*$^{\Delta E3/\Delta E3}$/*Mbnl3*$^{\Delta E2}$ mice displays both much stronger myotonia

Fig. 2. Mbnl3 deficits in conjunction with Mbnl1 loss results in a synergistic enhancement of myotonia. (A & B) The longest myotonic runs recorded from the EDL muscle of *Mbnl1*$^{\Delta E3/\Delta E3}$ (A) and *Mbnl1*$^{\Delta E3/\Delta E3}$/*Mbnl3*$^{\Delta E2}$ (B) mice (8.1 and 26 s, respectively) are shown. The bottom traces demonstrate waveform shape at an expanded time scale. The horizontal line indicates the region of the expanded trace. (C) Myotonic run lengths observed in the *Mbnl* genotypes tested are shown. (D) The EDL muscles from *Mbnl1*$^{\Delta E3/\Delta E3}$ and *Mbnl1*$^{\Delta E3/\Delta E3}$/*Mbnl3*$^{\Delta E2}$ mice produce significantly less maximal specific force (N/cm2) than wild type mice (asterisks, one-way ANOVA, p = 0.018). No force deficits were seen in *Mbnl2*$^{GT2/GT2}$ or *Mbnl3*$^{\Delta E2}$ mice. (E) Specific force/stimulation frequency curves for wild type, *Mbnl1*$^{\Delta E3/\Delta E3}$ and *Mbnl1*$^{\Delta E3/\Delta E3}$/*Mbnl3*$^{\Delta E2}$ mice. Reduced force production is seen at stimulation frequencies between 65–200 Hz in both *Mbnl1*$^{\Delta E3/\Delta E3}$ and *Mbnl1*$^{\Delta E3/\Delta E3}$/*Mbnl3*$^{\Delta E2}$ mice compared to wild type animals (n = 15, 8, 6, 7, 5, 6, 4 for wild type, *Mbnl1*$^{\Delta E3/\Delta E3}$, *Mbnl2*$^{GT2/GT2}$, *Mbnl3*$^{\Delta E2}$, *Mbnl1*$^{\Delta E3/\Delta E3}$/*Mbnl3*$^{\Delta E2}$, *Mbnl2*$^{GT2/GT2}$/*Mbnl3*$^{\Delta E2}$, and *Mbnl1*$^{+/\Delta E3}$/*Mbnl2*$^{GT2/GT2}$ mice). (F) *Mbnl1*$^{\Delta E3/\Delta E3}$/*Mbnl3*$^{\Delta E2}$ mice show myopathy of the EDL muscle. Muscle sections from *Mbnl1*$^{\Delta E3/\Delta E3}$/*Mbnl3*$^{\Delta E2}$ mice demonstrate centralized nuclei (asterisks), areas of atrophied fibers (arrow indicates two very small fibers), and regions of potential fibrosis (arrowheads). *Mbnl3*$^{\Delta E2}$ and *Mbnl2*$^{GT2/GT2}$ mice show no myopathic changes. *Mbnl1*$^{\Delta E3/\Delta E3}$ mice demonstrate mild myopathy with regions of muscle fibers containing centralized nuclei (asterisks). n = 3 muscles per genotype. Scale bar = 50 μm. (G) Clc-1 immunofluorescence is reduced in *Mbnl1*$^{\Delta E3/\Delta E3}$ and *Mbnl1*$^{\Delta E3/\Delta E3}$/*Mbnl3*$^{\Delta E2}$ mice. Confocal images of cryosectioned EDL muscles labeled for chloride channel (Clc-1) and nuclei (DAPI). Wild type, *Mbnl2*$^{GT2/GT2}$ and *Mbnl3*$^{\Delta E2}$ mice demonstrate the normal heterogeneity of Clc-1 labeling seen in confocal images of membrane channels in muscle. Preparations from *Mbnl1*$^{\Delta E3/\Delta E3}$ and *Mbnl1*$^{\Delta E3/\Delta E3}$/*Mbnl3*$^{\Delta E2}$ mice consistently demonstrated reduced Clc-1 labeling throughout muscle cross-sections (n = 3 muscles per genotype). Scale bar = 50 μm.

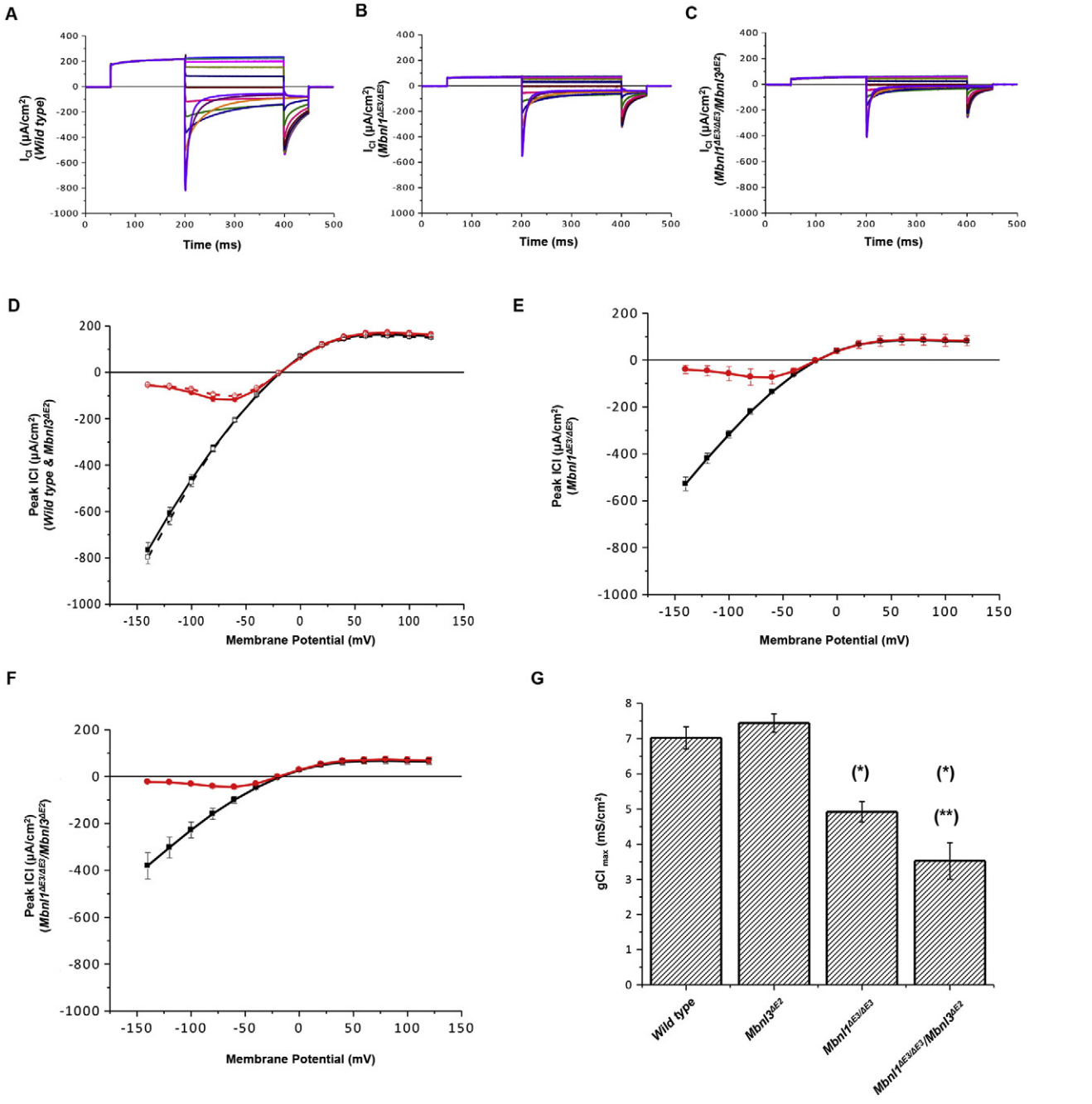

Fig. 3. Chloride currents are reduced in *Mbnl1*$^{\Delta E3/\Delta E3}$ and *Mbnl1*$^{\Delta E3/\Delta E3}$/*Mbnl3*$^{\Delta E2}$ foot muscles. (A–C) Family of chloride currents recorded in response to a three pulse protocol in wild type (A) *Mbnl1*$^{\Delta E3/\Delta E3}$ (B) and *Mbnl1*$^{\Delta E3/\Delta E3}$/*Mbnl3*$^{\Delta E2}$ (C) foot muscles are shown. Leak and capacitive current components were subtracted. The holding potential was set to −20 mV, which is equal to the Nernstian chloride equilibrium potential (E_{Cl}). The amplitude of the first (conditioning) pulse was +80 mV; the amplitude(s) of the second pulse (test pulses) ranged from 160 to −120 mV (in 20 mV steps); the third pulse amplitude was −60 mV. A period of 15 s was allowed between consecutive stimulations. (D–F) Voltage-dependence of the peak and steady state ICl in *Mbnl1*$^{\Delta E3/\Delta E3}$ and *Mbnl1*$^{\Delta E3/\Delta E3}$/*Mbnl3*$^{\Delta E2}$ foot muscles. I–V plots for the average peak (black symbols and lines) and steady state (red symbols and lines) ICl recorded from wild type (solid symbols; D), *Mbnl3*$^{\Delta E2}$ (open symbols; and D), *Mbnl1*$^{\Delta E3/\Delta E3}$ (E) and *Mbnl1*$^{\Delta E3/\Delta E3}$/*Mbnl3*$^{\Delta E2}$ (F) foot muscles are shown. Peak and steady-state currents were measured at the beginning and the end of the second pulse, respectively. (G) Maximal slope conductance (gCl_{max}) evaluated in wild type, *Mbnl1*$^{\Delta E3/\Delta E3}$, *Mbnl3*$^{\Delta E2}$ and *Mbnl1*$^{\Delta E3/\Delta E3}$/*Mbnl3*$^{\Delta E2}$ foot muscles. Columns represent the average maximal slope gCl recorded in response to hyperpolarizing pulses. The error bars are the SEM. One asterisk (*) indicates statistical significance ($p < 0.05$) with respect to wild type data; and two asterisks (**) indicate significance with respect to *Mbnl1*$^{\Delta E3/\Delta E3}$.

and show a much more significant shift of the average gCl_{max} to lower values (Fig. 4D). Furthermore, a significant number of fibers from *Mbnl1*$^{\Delta E3/\Delta E3}$/*Mbnl3*$^{\Delta E2}$ mice have extremely low values of gCl_{max}, reaching values as low as 1/7 of the average for wild type mice. Such values were never detected in the other 3 strains examined, and may readily explain why the *Mbnl1*$^{\Delta E3/\Delta E3}$/*Mbnl3*$^{\Delta E2}$ mice display much more pronounced myotonia than the *Mbnl1*$^{\Delta E3/\Delta E3}$ animals.

3.12. *Mbnl1*$^{\Delta E3/\Delta E3}$/*Mbnl3*$^{\Delta E2}$ Muscles Do Not Show an Enhancement in *Clc-1* Splice Defects or Further Reductions in *Clc-1* RNA Steady-State Levels When Compared to *Mbnl1*$^{\Delta E3/\Delta E3}$ Muscles

As the myotonia observed in DM1 has been hypothesized to result primarily from *Clc-1* splice errors and a concomitant reduction of RNA steady-state levels due to nonsense mediated decay of aberrantly

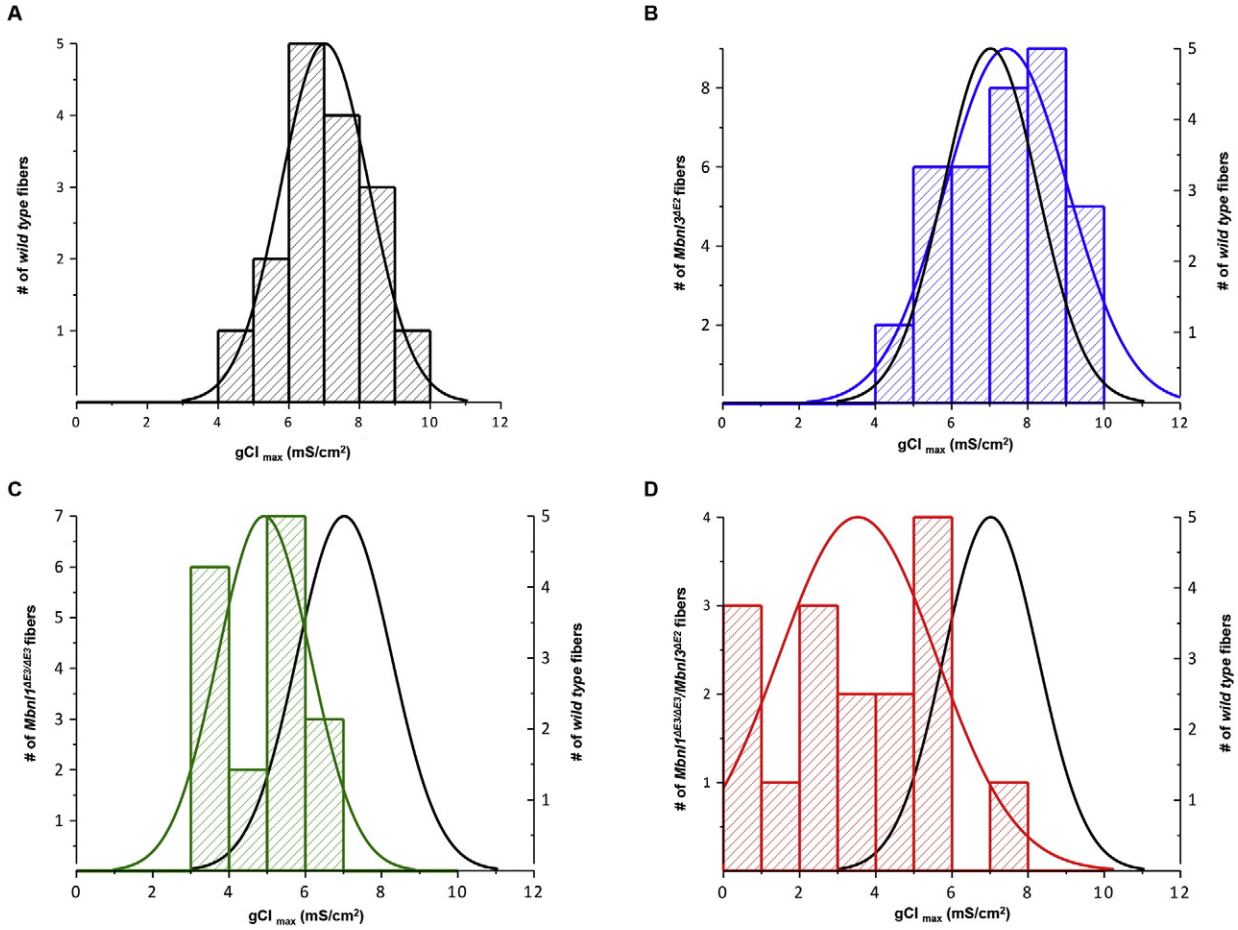

Fig. 4. *Mbnl1*$^{\Delta E3/\Delta E3}$/*Mbnl3*$^{\Delta E2}$ muscles show an increase in fibers with low gCl_{max} values. (A–D) Shown are histograms of the frequency distribution of gCl_{max} in fibers of wild type (A), *Mbnl3*$^{\Delta E2}$ (B), *Mbnl1*$^{\Delta E3/\Delta E3}$ (C), and *Mbnl1*$^{\Delta E3/\Delta E3}$/*Mbnl3*$^{\Delta E2}$ (D) mice, respectively. The bars are binned at 1 mS/cm^2. The solid lines represent fits to normal distributions. The fit to data from wild type mice (black solid line) is plotted superimposed with the data from other strains. The number of fibers used was 16, 37, 16 and 16 for panels A–D, respectively.

spliced *Clc-1* RNAs (Mankodi et al., 2002) we tested if *Clc-1* splice defects are enhanced in *Mbnl1*$^{\Delta E3/\Delta E3}$/*Mbnl3*$^{\Delta E2}$ mice. As expected, we observed enhanced (~50%) inclusion of *Clc-1* exon 7a in *Mbnl1*$^{\Delta E3/\Delta E3}$ muscles when compared with wild type muscles. Significantly, *Clc-1* exon 7a inclusion was not enhanced in *Mbnl1*$^{\Delta E3/\Delta E3}$/*Mbnl3*$^{\Delta E2}$ skeletal muscles when compared to *Mbnl1*$^{\Delta E3/\Delta E3}$ muscles (Fig. 5A). These results were confirmed by qPCR, which showed that the steady-state mRNA levels of *Clc-1* isoforms including exon 7a and exon 7 in *Mbnl1*$^{\Delta E3/\Delta E3}$/*Mbnl3*$^{\Delta E2}$ skeletal muscles was similar to that observed in *Mbnl1*$^{\Delta E3/\Delta E3}$ (Fig. S5A). To test the possibility that splice defects other than aberrant *Clc-1* exon 7a inclusion are enhanced in *Mbnl1*$^{\Delta E3/\Delta E3}$/*Mbnl3*$^{\Delta E2}$ mice, we checked exon inclusion for all *Clc-1* exons (Fig. S5B). Additional splice defects including retention of intron 2 and inclusion of exon 8a were observed in *Mbnl1*$^{\Delta E3/\Delta E3}$ skeletal muscles (Fig. 5A), but no enhancement of these splice errors was observed in *Mbnl1*$^{\Delta E3/\Delta E3}$/*Mbnl3*$^{\Delta E2}$ skeletal muscles when compared to *Mbnl1*$^{\Delta E3/\Delta E3}$ muscles. Consistent with the absence of an enhancement in *Clc-1* splice defects in *Mbnl1*$^{\Delta E3/\Delta E3}$/*Mbnl3*-$^{\Delta E2}$ skeletal muscles, steady-state *Clc-1* mRNA levels are similar in *Mbnl1*-$^{\Delta E3/\Delta E3}$ and *Mbnl1*$^{\Delta E3/\Delta E3}$/*Mbnl3*$^{\Delta E2}$ skeletal muscles (Fig. 5B). In addition, no difference in *Clc-1* hnRNA levels was observed in *Mbnl1*$^{\Delta E3/\Delta E3}$ and *Mbnl1*$^{\Delta E3/\Delta E3}$/*Mbnl3*$^{\Delta E2}$ skeletal muscles (Figs. 5C and S5C & D). These data support the hypothesis that aberrant chloride channel splicing is necessary but insufficient for myotonia to fully manifest in *Mbnl1*$^{\Delta E3/\Delta E3}$/*Mbnl3*$^{\Delta E2}$ mice.

3.13. *Clc-1* RNA Translation is Altered in *Mbnl1*$^{\Delta E3/\Delta E3}$/*Mbnl3*$^{\Delta E2}$ Muscles

The observation that *Mbnl1*$^{\Delta E3/\Delta E3}$/*Mbnl3*$^{\Delta E2}$ muscles do not display enhancement in *Clc-1* splice defects or differences in mRNA steady-state levels when compared with *Mbnl1*$^{\Delta E3/\Delta E3}$ muscles suggest that Clc-1 expression might be regulated at the translation level. A recent study has shown that $Mbnl3_{38kD}$ co-fractionates with polysomes in C2C12 cells, suggesting that $Mbnl3_{38kD}$ may be involved in translation of $Mbnl3_{38kD}$ target RNAs (Poulos et al., 2013). In contrast, Mbnl1 has been shown to associate with smaller mRNP particles, but not with polysomes in HeLa cells (Onishi et al., 2008). To clarify whether Mbnl1 associates with polysomes in mouse skeletal muscle, we performed polysome analysis using sucrose gradient fractionation. As reported for HeLa cells, we found that the majority of Mbnl1 co-fractionates with smaller mRNP particles. However in skeletal muscle Mbnl1 was also detected in polysome fractions (Fig. S6). This observation was confirmed by polysome disruption with EDTA treatment, which resulted in a shift of Mbnl1 in polysome factions to lower density fractions (Fig. S6). These data suggested that Mbnl1 and Mbnl3 might be involved in the translational regulation of *Clc-1* mRNA. Polyribosomes were therefore prepared using soleus muscles dissected from wild type (n = 4), *Mbnl1*$^{\Delta E3/\Delta E3}$ (n = 5), *Mbnl3*$^{\Delta E2}$ (n = 3) and *Mbnl1*$^{\Delta E3/\Delta E3}$/*Mbnl3*$^{\Delta E2}$ (n = 3) mice on 20–50% density sucrose gradient and polyribosome profiles were analyzed by A_{254} absorbance (Fig. 6A) and non-denaturing agarose gel electrophoresis (Fig. S7). Relative *Clc-1* mRNA distribution in each of the 16 polysome sucrose gradient fractions from wild type, *Mbnl1*$^{\Delta E3/\Delta E3}$, *Mbnl3*$^{\Delta E2}$ and *Mbnl1*$^{\Delta E3/\Delta E3}$/*Mbnl3*$^{\Delta E2}$ soleus muscles was analyzed by qPCR. Relative *Clc-1* mRNA distribution was not significantly different in *Mbnl1*$^{\Delta E3/\Delta E3}$ *and Mbnl3*$^{\Delta E2}$ muscles when compared to wild type muscles. However *Mbnl1*$^{\Delta E3/\Delta E3}$/*Mbnl3*$^{\Delta E2}$ skeletal muscles showed a very distinctive *Clc-1* mRNA distribution pattern when compared to wild type and *Mbnl1*$^{\Delta E3/\Delta E3}$ muscles and demonstrated that *Clc-1* mRNA is highly enriched in fraction numbers 6 and 7 that correspond to monosomes and the first polysomes respectively as shown in

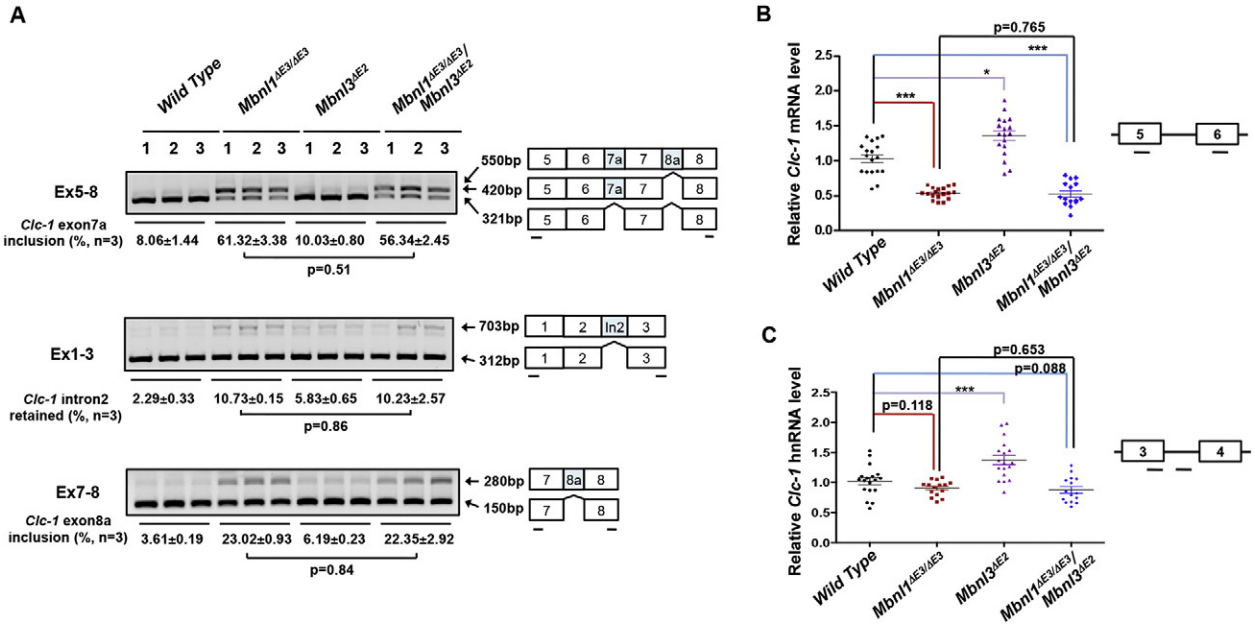

Fig. 5. Chloride channel RNA splicing and steady-state RNA levels are not significantly different in $Mbnl1^{\Delta E3/\Delta E3}$ and $Mbnl1^{\Delta E3/\Delta E3}/Mbnl3^{\Delta E2}$ muscles. (A) Alternative splicing was analyzed for *Clc-1* in wild type, $Mbnl1^{\Delta E3/\Delta E3}$, $Mbnl3^{\Delta E2}$, and $Mbnl1^{\Delta E3/\Delta E3}/Mbnl3^{\Delta E2}$ soleus muscles (n = 3) by RT-PCR. Exon numbers, position of primers and expected band sizes are indicated. The alternatively spliced exons are shown as blue boxes. Exon numbers are annotated based on Refseq from UCSC genome browser (NCBI37/mm9). Band intensities were quantified by densitometry. No statistical significance was observed for *Clc-1* alternative splicing between $Mbnl1^{\Delta E3/\Delta E3}$ and $Mbnl1^{\Delta E3/\Delta E3}/Mbnl3^{\Delta E2}$ soleus muscles. (B–C) RNA from wild type, $Mbnl1^{\Delta E3/\Delta E3}$, $Mbnl3^{\Delta E2}$, and $Mbnl1^{\Delta E3/\Delta E3}/Mbnl3^{\Delta E2}$ soleus muscles (n = 6) were subjected to qPCR to measure *Clc-1* mRNA (B) and hnRNA (C) steady-state levels. *Clc-1* mRNA and hnRNA levels were normalized to that of *Gapdh*. Location of *Clc-1* exon–exon boundary spanning primers and exon–intron boundary spanning primers used for mRNA and hnRNA level measurements are shown. PCR amplification in the absence of reverse transcriptase was used to confirm the absence of genomic DNA contaminants (Fig. S5). Error bars represent standard error of mean (SEM). Each sample was replicated in triplicate. p-values were determined by paired student's *t*-test. * and *** indicates $p < 0.05$ and $p < 0.0001$, respectively.

the A_{254} traces of total RNA distribution (Fig. 6A & B). To further test whether the *Clc-1* polysome distribution pattern observed in $Mbnl1^{\Delta E3/\Delta E3}/Mbnl3^{\Delta E2}$ mice is specific, we analyzed the *Clc-1* mRNA distribution pattern subsequent to EDTA treatment by qPCR. As expected, EDTA treatment resulted in a shift of the *Clc-1* mRNAs to lighter fractions by polysome disruption (Fig. 6C). Western blot analysis did not show significant differences in Gapdh levels in the mouse genotypes studied (Fig. S8). Consistent with this observation relative *Gapdh* mRNA distribution in the 16 polysome sucrose gradient fractions from wild type, $Mbnl1^{\Delta E3/\Delta E3}$, $Mbnl3^{\Delta E2}$ and $Mbnl1^{\Delta E3/\Delta E3}/Mbnl3^{\Delta E2}$ skeletal muscles were not significantly different (Fig. 6D). To determine whether the distinct *Clc-1* mRNA distribution pattern in $Mbnl1^{\Delta E3/\Delta E3}/Mbnl3^{\Delta E2}$ skeletal muscles is also observed with the overexpression of *CUGexp* RNA *in vivo*, we analyzed the HSA^{LR} mouse model for myotonic dystrophy, which expresses 250 CUG repeats located in the 3′ UTR of the human skeletal actin transgene that results in the aberrant sequestration of the Mbnl proteins (Mankodi et al., 2002; Lin et al., 2006). As expected, we observed enhanced inclusion of *Clc-1* exon 7a in HSA^{LR} muscles when compared to wild type muscles (Fig. 6E). However, in contrast to a 7 fold increase in $Mbnl1^{\Delta E3/\Delta E3}/Mbnl3^{\Delta E2}$ skeletal muscles (Fig. S5B), the HSA^{LR} muscles showed a 2.6 fold increase in the steady-state mRNA levels of the *Clc-1* isoforms including exon 7a when compared to wild type muscles. Consistent with this observation, steady-state *Clc-1* mRNA levels in the HSA^{LR} skeletal muscles were reduced by ~30% when compared to wild type muscles (Fig. 6F), in contrast to the ~50% reduction in $Mbnl1^{\Delta E3/\Delta E3}/Mbnl3^{\Delta E2}$ muscles (Fig. 5B). The reduced severity of *Clc-1* RNA processing defects may reflect the less than complete sequestration of the Mbnl proteins by *CUGexp* in the HSA^{LR} mice. Polyribosome profiles from ~2 month old wild type (n = 6) and HSA^{LR} (n = 6) soleus muscles were analyzed by A_{254} absorbance (Fig. 6G) and relative *Clc-1* mRNA distribution in each of the 16 polysome sucrose gradient fractions was analyzed by qPCR (Fig. 6H). Similar to $Mbnl1^{\Delta E3/\Delta E3}/Mbnl3^{\Delta E2}$ skeletal muscles, *Clc-1* mRNA was significantly enriched in fraction number 7 in HSA^{LR} skeletal muscle when compared to wild type muscle (Fig. 6H). These data strongly

Fig. 6. Clc-1 expression is regulated at the translational level in $Mbnl1^{\Delta E3/\Delta E3}/Mbnl3^{\Delta E2}$ muscles.(A) Each aliquot (containing 13 OD at A260nm) of polyribosomal preparations from wild type (n = 4), $Mbnl1^{\Delta E3/\Delta E3}$ (n = 5), $Mbnl3^{\Delta E2}$ (n = 3), and $Mbnl1^{\Delta E3/\Delta E3}/Mbnl3^{\Delta E2}$ (n = 3) soleus muscles was fractionated by centrifugation at 40,000 rpm for 2 h at 4 °C using a 20%–50% w/w linear density gradient of sucrose. A_{254} traces of total RNA distributions are shown. Gradient fraction numbers, 40S, 60S, 80S and polysomes are indicated.(B) cDNAs were prepared using equal volumes of RNA from each of the 16 sucrose gradient fractions. *Clc-1* mRNA distribution in each fraction derived from wild type, $Mbnl1^{\Delta E3/\Delta E3}$, $Mbnl3^{\Delta E2}$, and $Mbnl1^{\Delta E3/\Delta E3}/Mbnl3^{\Delta E2}$ soleus muscles was analyzed by qPCR.(C) *Clc-1* mRNA distribution in each fraction analyzed by qPCR from muscle extracts treated with EDTA.(D) *Gapdh* mRNA distribution in each of the 16 sucrose gradient fractions from wild type, $Mbnl1^{\Delta E3/\Delta E3}$, $Mbnl3^{\Delta E2}$ and $Mbnl1^{\Delta E3/\Delta E3}/Mbnl3^{\Delta E2}$ soleus muscles was analyzed by qPCR.Data are plotted as percentages of the total mRNA on the gradient. Error bars represent the standard error of mean (SEM). p-Values were calculated using two-way ANOVA multiple comparisons. *, *** and **** indicates $p < 0.05$, $p < 0.0001$ and $p < 0.00001$, respectively.(E) Alternative splicing was analyzed for *Clc-1* in wild type and HSA^{LR} soleus muscles (n = 3) by RT-PCR. Exon numbers, position of primers and expected band sizes are indicated. The alternatively spliced exons are shown as blue boxes. Exon numbers are annotated based on Refseq from UCSC genome browser (NCBI37/mm9). Band intensities were quantified by densitometry. The state-state mRNA level of *Clc-1* isoforms including exon 7a and exon 7 in wild type and HSA^{LR} mice (n = 3) was measured by qPCR. Expression levels of *Clc-1* isoforms including exon 7a were normalized to that of *Gapdh*. Error bars represent standard error of mean (SEM). Each sample was replicated in triplicate. p values were determined by paired Student's *t*-test. ** indicate $p<0.001$.(F) RNA from wild type and HSA^{LR} soleus muscles (n = 3) were subjected to qPCR to measure *Clc-1* mRNA steady-state levels. *Clc-1* mRNA levels were normalized to that of *Gapdh*. Error bars represent standard error of mean (SEM). Each sample was replicated in triplicate. p-values were determined by paired Student's *t*-test. *** indicates $p<0.0001$.(G) A_{254} traces of total RNA distributions from wild type and HSA^{LR} soleus muscles are shown. Gradient fraction numbers, 40S, 60S, 80S and polysomes are indicated.(H) *Clc-1* mRNA distribution in each of the 16 sucrose gradient fractions from wild type and HSA^{LR} soleus muscles (n = 6) was analyzed by qPCR. Error bars represent the standard error of mean (SEM). p-Values were calculated using two-way ANOVA multiple comparisons. ** indicates $p < 0.001$.

suggest that Clc-1 expression is regulated at the translational level and that both Mbnl1 and Mbnl3 are required for optimal *Clc-1* mRNA translation. Recent study has demonstrated that depletion of Mbnl proteins leads to misregulation of alternative polyadenylation (APA) events (Batra et al., 2014) and another study has reported that depletion of Mbnl1 and 2 results in mislocalization of many mRNA (Wang et al., 2012), implicating the Mbnl proteins in regulation of APA and localization of mRNAs. As these events could impact translation, we checked whether poly(A) site shifts occurred in *Clc-1* mRNA in *Mbnl1*$^{\Delta E3/\Delta E3}$/*Mbnl3*$^{\Delta E2}$ skeletal muscles. We identified a novel proximal poly(A) start site in the 3′ UTR of *Clc-1* gene and a distal poly(A) start site downstream of the *Clc-1* 3′ UTR both by restriction enzyme digestion and sequencing (Figs. S9 & S10). However, no significant poly(A) site shift was observed in *Mbnl1*$^{\Delta E3/\Delta E3}$/*Mbnl3*$^{\Delta E2}$ skeletal muscles when compared to wild type muscles (Fig. S11). Therefore, it is unlikely that the translation defects observed in *Mbnl1*$^{\Delta E3/\Delta E3}$/*Mbnl3*$^{\Delta E2}$ skeletal muscles result from alternative poly(A) selection. To

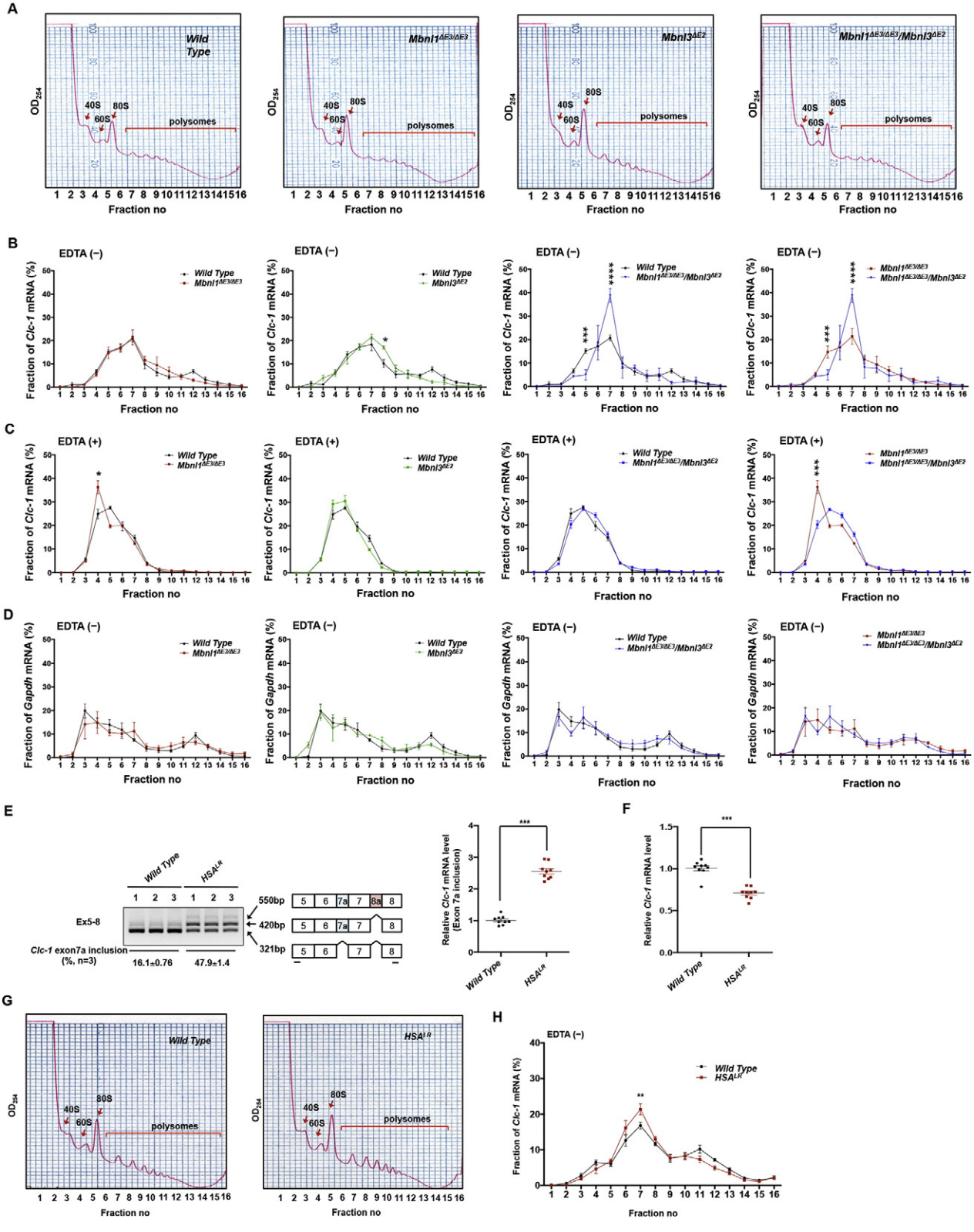

test the possibility that mislocalization of *Clc-1* mRNA in *Mbnl1*$^{\Delta E3/\Delta E3}$/*Mbnl3*$^{\Delta E2}$ skeletal muscles leads to a translation defect, we measured the relative *Clc-1* mRNA levels in subcellular fractions that were isolated from wild type and *Mbnl1*$^{\Delta E3/\Delta E3}$/*Mbnl3*$^{\Delta E2}$ skeletal muscles. However, we observed no significant difference in the *Clc-1* mRNA levels in the nuclear, cytoplasmic and membrane fractions from wild type and *Mbnl1*$^{\Delta E3/\Delta E3}$/*Mbnl3*$^{\Delta E2}$ mice (Fig. S12).

3.14. Mbnl1 and Mbnl3 Bind Clc-1 mRNA

We analyzed *Clc-1* mRNA sequences to identify the putative *Mbnl1* and *Mbnl3* binding sites by using SFmap (Akerman et al., 2009; Ho et al., 2004; Paz et al., 2010; Poulos et al., 2013). We identified 21 and 34 binding sites in the coding region, whereas only 2 and 3 binding sites were found in 3′ UTR for Mbnl1 and Mbnl3, respectively (Fig. S3A). We then determined whether Mbnl1 and Mbnl3 directly binds *Clc-1* mRNAs (3545nts) by using *in vitro* RNA binding assays. ^{32}P-labeled *Clc-1* (1–1994), *Clc-1* (1945–3545) and *Clc-1* (3′ UTR) transcripts showed similar binding to recombinant His-Mbnl1 and His-Mbnl3, but not to GST. As expected, however, ^{32}P-labeled *Clc-1* (3′ UTR) transcripts showed very weak binding to Mbnl1 and Mbnl3 proteins when compared to *Clc-1* (1–1994) and *Clc-1* (1945–3545) transcripts (Fig. S13B). Neither His-Mbnl1 nor His-Mbnl3 bound to ^{32}P-labeled *Gapdh* transcripts, indicating that the binding between *Clc-1* mRNA and Mbnl1 and Mbnl3 is specific (Fig. 7A).

3.15. Mbnl1 and Mbnl3 Demonstrate RNA Regulated Association with Hsp70 and eEF1A

As we observed that the depletion of Mbnl1 and Mbnl3 results in *Clc-1* mRNA accumulation in monosomes and the first polysome fractions (Fig. 6), we tested if these proteins act as adaptors to recruit factors required for translation. To identify proteins associated with Mbnl3, we established cell lines that stably express Flag-tagged Mbnl3. We then purified and identified Mbnl3-associated factors by Mass spectrometry analysis (Fig. 7B). The identified Mbnl3-associated factors were compared with the Mbnl1-associated factors (Paul et al., 2011). We found that two factors, Hsp70 and eEF1A, associate with both Mbnl1 (Fig. S14) and Mbnl3 (Fig. 7B) and the interaction of these factors with Mbnl1 and Mbnl3 was validated by coimmunoprecipitation (Fig. 7C & D). To check whether RNA mediates these interactions, we performed coimmunoprecipitation assays both in the presence and absence of RNase A. Interestingly, the interaction between Hsp70 and Mbnl1 and Mbnl3 increased in the presence of RNase A. A similar increase in the interaction between eEF1A and both Mbnl1 and Mbnl3 was observed in the presence of RNase A (Fig. 7C & D). Our data suggest that the Mbnl proteins may behave as adaptors that serve to recruit protein cargoes to target RNAs. Proteins bound to Mbnl 1 and Mbnl3, which either remains bound to the Mbnl proteins upon target RNA binding or that are released at the site of target RNA binding, can serve to increase the local concentration of these proteins at the site of target RNA binding. To test this idea, we performed coimmunoprecipitation assays in the presence of added *CUG* repeat-encoding RNAs, which are known to strongly bind both the Mbnl1 and the Mbnl3 proteins. We observed that binding of Hsp70 to the Mbnl proteins decreases as the amount of the *CUG* transcripts increase (Fig. 7E & F). Binding to Hsp70 decreased more sharply for Mbnl3 when compared to Mbnl1 in the presence of *CUG* repeats (Fig. 7E & F). Thus the enhanced interaction between the cargo protein, Hsp70 and Mbnl1 and Mbnl3 in the presence of RNase may reflect such reversible and competitive binding. The kinetics of cargo protein release may however be influenced by the binding affinity or location of the binding sites on the target RNAs. These results suggest that Hsp70 and Mbnl-target RNAs bind reversely and competitively to Mbnl protein. As both Mbnl1 and Mbnl3 bind *Clc-1* mRNAs and depletion of these proteins results in an accumulation of *Clc-1* mRNA with monosomes and the first polysome fractions, our data suggests that Mbnl1 and Mbnl3 binding to *Clc-1* mRNA engaged in ribosomes may facilitate an increase in the local concentration of Hsp70 and eEF1A to enhance translation (Fig. 7G).

4. Discussion

To test the role of the Mbnl family of proteins in skeletal muscle function we have developed and examined transgenic mouse strains that show single and combinatorial deficits in the three muscleblind proteins, Mbnl1, Mbnl2 and Mbnl3. In contrast with the *Mbnl1*$^{\Delta E3/\Delta E3}$ mice, which have previously been described to recapitulate some features of DM1 muscle disease (Kanadia et al., 2003), *Mbnl2*$^{GT2/GT2}$ and *Mbnl3*$^{\Delta E2}$ mice are viable and show no overt skeletal muscle pathology. Dual deficits of Mbnl1 and Mbnl2 results in a lethal phenotype reminiscent of the increase in the spontaneous abortion rate reported in DM1. An increase in the severity of the skeletal muscle disease observed with the depletion of both Mbnl1 and Mbnl3 manifests as a synergistic enhancement of myotonia, reductions in force production and alterations in histopathology observed as an increase in atrophic fibers with a potential for increased fibrosis and central nuclei. Consistent with enhanced myotonia, examination of chloride channel function demonstrates both a reduction in the magnitude of average peak ICl in fibers from *Mbnl1*$^{\Delta E3/\Delta E3}$/*Mbnl3*$^{\Delta E2}$ mice and a significant increase in the numbers of fibers having extremely low values of gCl_{max} that approach ~1 mS/cm^2 as compared with an average of 7 mS/cm^2 for wild type mice. The enhancement in chloride channel dysfunction in *Mbnl1*$^{\Delta E3/\Delta E3}$/*Mbnl3*$^{\Delta E2}$ mice does not result from an increase in the severity of *Clc-1* RNA splice errors, a further decrease in *Clc-1* RNA steady-state levels, altered polyA start sites or *Clc-1* mislocalization when compared with *Mbnl1*$^{\Delta E3/\Delta E3}$ animals, but rather from *Clc-1* mRNA translation defects. Our data suggest that Mbnl1 and Mbnl3 act as adaptors to recruit Hsp70 and eEF1A to *Clc-1* RNA engaged with ribosomes to facilitate translation.

The muscleblind protein family encodes two pairs of zinc fingers, each containing three cysteines and one histidine residue, with other regions being conserved to varying degrees (Fardaei et al., 2002). These proteins show specialized patterns of expression, with MBNL1 levels remaining unchanged during myoblast differentiation and MBNL2 and MBNL3 levels showing elevated expression in myoblasts and diminishing with differentiation (Holt et al., 2009). *Mbnl1* and *Mbnl2* RNAs are detected in adult muscle, heart, brain, kidney, liver and pancreas. *Mbnl3* RNA expression is low in adult tissues (Fardaei et al., 2002). All three proteins sequester strongly in CUG foci in DM1 cells (Fardaei et al., 2002).

As we do not observe significant mortality in litters derived from *Mbnl1*$^{+/\Delta E3}$ X *Mbnl2*$^{+/GT2}$ crosses, our data support the model that combinatorial deficits of Mbnl1 and Mbnl2 results in an embryonic lethal phenotype. These data are reminiscent of the high rate of fetal loss resulting from spontaneous abortion that is documented in DM1 (Jaffe et al., 1986). Thus complete sequestration of the MBNL1 and MBNL2 proteins in CUG foci may lead to embryonic lethality with less complete sequestration in various cell types and organ systems leading to viable but impaired individuals exhibiting a variety of pathological features (Charizanis et al., 2012; Lee et al., 2013).

Mbnl3 and Mbnl1 loss results in a synergistic interaction manifesting as enhanced myotonia, diminished force production and a histopathology of central nuclei, atrophic fibers and regions of potential fibrosis, in skeletal muscle. These results are particularly intriguing, as Mbnl3 loss does not result in significant muscle pathology. To examine the mechanism underlying this synergy we focused our studies on the 4 to 10 fold enhancement in myotonia observed in the limb muscles of mice lacking Mbnl1 and Mbnl3 when compared to animals lacking only Mbnl1. As previous studies have implicated chloride current deficits in the development of myotonia in the *HSA*^{LR} mouse model and mice lacking Mbnl1 (Kanadia et al., 2003; Mankodi et al., 2002), we

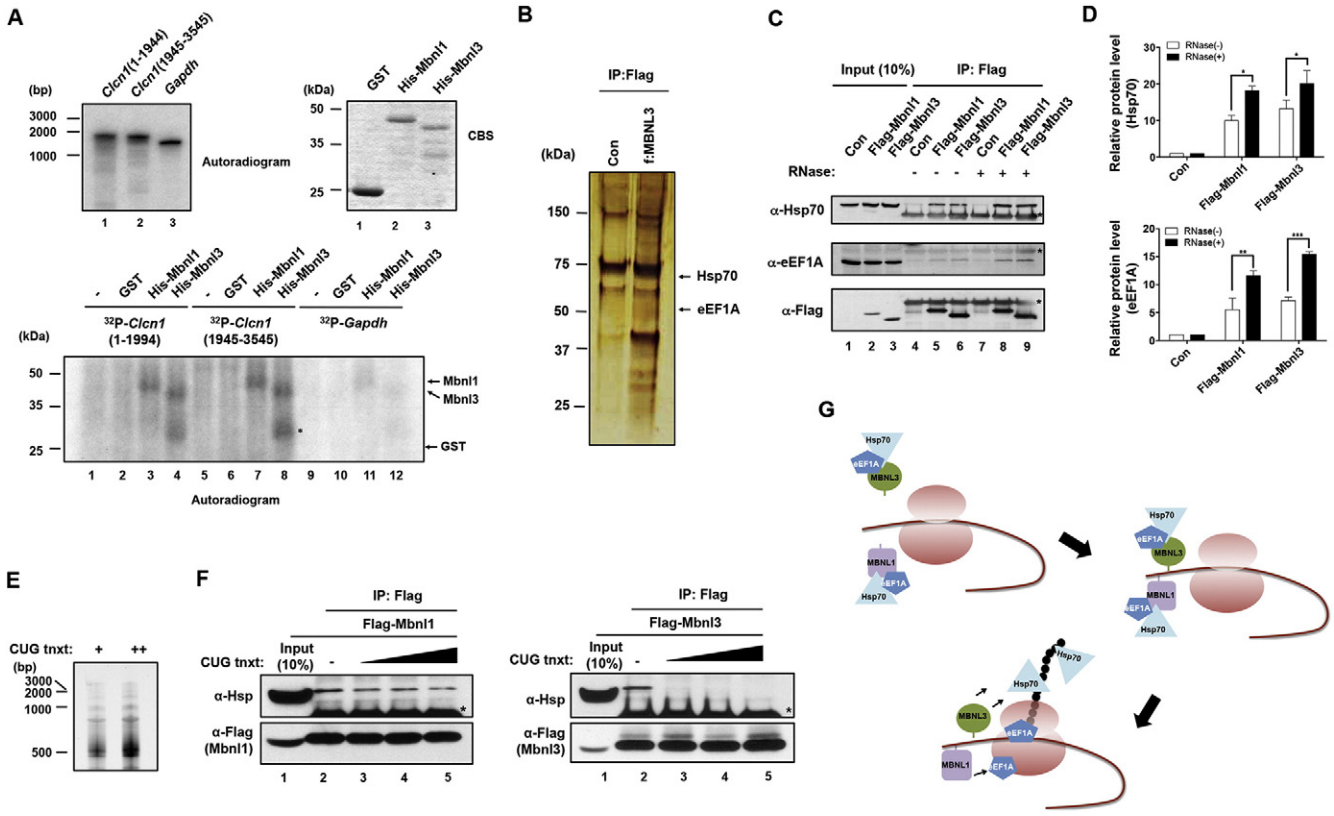

Fig. 7. Mbnl1 and Mbnl3 bind *Clc-1* mRNA and associate with Hsp70 and eEF1A. (A) *In vitro* transcribed ^{32}P-labeled *Clc-1* (1–1944) and *Clc-1* (1945–3545) RNAs (*Clc-1* mRNA: 3545 nts) were incubated with either recombinant His-Mbnl1 or Mbnl3 to test binding of *Clc-1* RNA with Mbnl1 and Mbnl3. Recombinat GST protein and ^{32}P-labeled *Gapdh* transcripts were used as controls for the Mbnl proteins and ^{32}P-labeled *Clc-1* transcripts, respectively. The radioactive RNA-protein complex was visualized by autoradiography. Asterisk (*) shows non-specific binding. ^{32}P-labeled *Clc-1* (1–1944), *Clc-1* (1945–3545) and *Gapdh* transcripts were visualized by 5% acrylamide gel electrophoresis and autoradiography. Purified recombinant GST, His-Mbnl1 and His-Mbnl3 were confirmed by coommassie blue staining (CBS). RNA and protein sizes are indicated. (B) Affinity purification of Mbnl3-interacting proteins. Flag-tagged Mbnl3 was stably expressed in HEK293 cells and subjected to immunoprecipitation utilizing anti-Flag antibodies. The copurified proteins were separated by 4–20% gradient SDS-PAGE. Specific bands were excised and analyzed by LC/MS–MS analysis. Identified Mbnl3-interacting proteins are indicated. (C–D) Interaction of endogenous Hsp70 and eEF1A with Mbnl3. One half of the whole cell extracts prepared from the control and stable cell lines expressing Flag-Mbnl3 were pre-treated with RNase A (1 mg/ml) for 15 min at 37 °C. Untreated and RNase A treated extracts were immunoprecipitated with anti-Flag antibodies and analyzed by Western blotting using anti-Flag, Hsp70 and eEF1A antibodies as indicated. Band intensities were quantitated by densitometry and normalized to that of the immunoprecipitated Mbnl proteins with anti-Flag antibodies. Asterisks indicate nonspecific bands. Lanes 1–3 represents 10% of the input. Error bars represent the standard error of mean (SEM). p-Values were calculated using two-way ANOVA multiple comparisons. *, ** and *** indicates $p < 0.05$, $p < 0.001$ and $p < 0.0001$, respectively. (E–F) One half of the whole cell extracts prepared from the stable cell lines expressing Flag-Mbnl1 or Flag-Mbnl3 were pre-treated with various concentration (200, 400 and 800 ng) of *in vitro* transcribed CUG transcripts (E) for 30 min at 4 °C. Untreated and CUG transcript-treated extracts were immunoprecipitated with anti-Flag antibodies and analyzed by Western blotting using anti-Flag, Hsp70 antibody (F). Asterisks indicate IgG heavy chain. Lanes 1 represents 10% of the input. (G) Clc-1 expression is regulated at the translation level by Mbnl1 and Mbnl3.

examined the function of these channels in mice lacking either Mbnl1 or Mbnl3 and in animals deficient in both Mbnl1 and Mbnl3. In partial agreement with previous results obtained in young mice (Lueck et al., 2007), we found that loss of Mbnl1 in muscle fibers from adult mice resulted in a ~33% decrease in ICl. We further discovered that the dual loss of Mbnl1 and Mbnl3 results in a more severe decrease in ICl to ~49% of its normal value. Comparative examination of the frequency distribution of gCl_{max} in muscle fibers from wild type and transgenic mice lacking Mbnl1, Mbnl3 or both Mbnl1 and Mbnl3, shows that only mice lacking Mbnl3 are indistinguishable from wild type animals. In contrast, fibers lacking Mbnl1 show a broader gCl_{max} distribution shifted towards lower values. Strikingly, fibers lacking both Mbnl1 and Mbnl3 demonstrate a more pronounced shift, and a further widening in the frequency distribution. Specifically, in muscles lacking both Mbnl1 and Mbnl3, a significant number of muscle fibers analyzed show gCl_{max} values that approach ~1 mS/cm^2, compared with an average value of 7 mS/cm^2 found in wild type mice, and with approximately one-third of the population displaying gCl_{max} below the lowest value found in wild type controls. We surmise that such fibers, which are significantly more prevalent in $Mbnl1^{\Delta E3/\Delta E3}/Mbnl3^{\Delta E2}$ mice, explain the stronger myotonia in $Mbnl1^{\Delta E3/\Delta E3}/Mbnl3^{\Delta E2}$ animals when compared with $Mbnl1^{\Delta E3/\Delta E3}$ mice.

ICl with aberrant features are not observed in $Mbnl1^{\Delta E3/\Delta E3}$ and $Mbnl1^{\Delta E3/\Delta E3}/Mbnl3^{\Delta E2}$ mice. Rather, comparison of the reduction in $[\text{peak ICl}]_{max}$ and gCl_{max} observed in $Mbnl1^{\Delta E3/\Delta E3}$ and $Mbnl1^{\Delta E3/\Delta E3}/Mbnl3^{\Delta E2}$ mice with the semi-quantitative immunohistochemical analysis of Clc-1 in these animals support the hypothesis that the decrease in ICl in these two strains may be at least in part a consequence of the reduced expression of functional Clc-1 channels. In this regard it is of interest to note that the diminished chloride currents in DM1 patients and in the HSA^{LR} mice, have been hypothesized to result as a consequence of decreased Clc-1 levels reflecting nonsense mediated decay of aberrantly spliced *Clc-1* RNAs (Mankodi et al., 2002). Thus, we examined if *Clc-1* splice defects were enhanced or if *Clc-1* RNA steady-state levels were significantly decreased in $Mbnl1^{\Delta E3/\Delta E3}/Mbnl3^{\Delta E2}$ muscles when compared with $Mbnl1^{\Delta E3/\Delta E3}$ muscles. No significant differences in either the *Clc-1* splice patterns or RNA steady-state levels were observed in either lower limb or foot muscles lacking both Mbnl3 and Mbnl1 when compared with corresponding muscles lacking Mbnl1. Consistent with this observation, Clc-1 splicing defects were not observed in $Mbnl3^{\Delta E2}$ muscles. Thus reduction in functional Clc-1 levels in $Mbnl1^{\Delta E3/\Delta E3}/Mbnl3^{\Delta E2}$ muscles when compared to $Mbnl1^{\Delta E3/\Delta E3}$ muscles can reflect events resulting from Mbnl3 loss, which may in

combination with one or more deficits resulting from Mbnl1 depletion, synergize to facilitate diminished chloride channel function.

Previous studies have demonstrated that unlike the truncated 27 kDa Mbnl3 isoform, the full-length 38 kDa Mbnl3 isoform cofractionates with polysomes (Poulos et al., 2013). In this study, we observe that a fraction of the Mbnl1 protein also cofractionates with polysomes. These observations suggested that the enhanced reduction of Clc-1 function in *Mbnl1*$^{\Delta E3/\Delta E3}$/*Mbnl3*$^{\Delta E2}$ muscles may result from *Clc-1* mRNA translation defects. Polyribosome profiling analysis shows that Mbnl1 and Mbnl3 depletion results in significant accumulation of *Clc-1* mRNA in gradient fractions corresponding to the monosome and the first poylsome when compared to wild type and *Mbnl1*$^{\Delta E3/\Delta E3}$ animals. Interestingly, although ~57% of *Clc-1* mRNA in *Mbnl1*$^{\Delta E3/\Delta E3}$/*Mbnl3*$^{\Delta E2}$ muscles is associated with monosomes and single polysomes, 37% of the *Clc-1* mRNA associated with heavier polysome fractions, indicating that this translation defect does not completely block the *Clc-1* RNA transition to heavier polysome fractions. Thus rather than an all or none effect this defect may increase the chance of diminished Clc-1 protein production and serve to explain the increase in the number of fibers showing very low chloride currents in *Mbnl1*$^{\Delta E3/\Delta E3}$/*Mbnl3*$^{\Delta E2}$ muscles.

The translation defects observed for the *Clc-1* mRNA appear to be specific as similar alterations were not observed for the *Gapdh* mRNA. Consistent with this idea, we observe that Mbnl1 and Mbnl3 specifically bind to the *Clc-1* mRNA when examined using *in vitro* RNA binding assays. As depletion of either Mbnl1 or Mbnl3 does not show the prominent defects in *Clc-1* RNA distribution on polysome fractions observed in muscles lacking both proteins, it is likely that Mbnl1 and Mbnl3 may have partially redundant functions in *Clc-1* mRNA translation regulation. It is therefore conceivable that translation related factors associated with both Mbnl1 and Mbnl3 could be involved in the translation regulation of the *Clc-1* mRNA.

In the next set of experiments we identified Hsp70 and eEF1A as Mbnl1 and Mbnl3-interacting factors. These results are significant because Hsp70 is known to play a key role in protein synthesis by association with nascent polypeptides (Beckmann et al., 1990). As the nascent polypeptide chain emerges into the cytosol, interaction with Hsp70 is crucial for the continuous transport of the polypeptide through the ribosome channel into the cytosol (Nelson et al., 1992). Hsp70 deficits can therefore cause the nascent polypeptide to interfere with translation by clogging the ribosome channel. Thus Hsp70 deficits can perturb protein synthesis at the translocation step, which can result in reduced accessibility of the EF1A-aminoacyl-tRNA complex to the ribosome (Nelson et al., 1992). In this context, it is interesting to speculate on the mechanism by which Clc-1 expression is regulated in *Mbnl1*$^{\Delta E3/\Delta E3}$/*Mbnl3*$^{\Delta E2}$ muscles. As Mbnl1 and Mbnl3 bind *Clc-1* mRNA specifically and because the interaction between Mbnl1 and Mbnl3 with Hsp70 and eEF1A increases subsequent to treatment of RNase A or an increase in the concentration of CUG repeat encoding transcripts, Mbnl1 and Mbnl3 may act as adaptors, that serve to increase the local concentration of Hsp70 and eEF1A on *Clc-1* mRNAs engaged with ribosomes (Fig. 7C–G). Therefore, Mbnl1 and Mbnl3 depletion can result in the reduction of the local concentration of Hsp70 and eEF1A and consequently shift the *Clc-1* mRNA distribution towards the lighter polysome fractions. As these events may serve to shift the equilibrium towards less efficient translation rather than a complete stalling of translation, they can provide an explanation for the increase in the frequency with which muscle fibers with low chloride currents are encountered in *Mbnl1*$^{\Delta E3/\Delta E3}$/*Mbnl3*$^{\Delta E2}$ muscles. Taken together our data demonstrate that Mbnl1 and Mbnl3 deficits profoundly enhance myotonia and that the mechanisms driving this enhancement are not only *Clc-1* splice errors resulting from Mbnl1 loss, but also *Clc-1* translation defects occurring from the dual loss of Mbnl1 and Mbnl3. Importantly, as both *Clc-1* splice defects and an aberrant accumulation of *Clc-1* RNA on monosomes and the first polysomes is observed in the *HSA*^{LR} DM1 model, where a similar increase in a subpopulation of muscle fibers with low chloride currents has been reported (DiFranco et al., 2013), our data demonstrate that splice defects work coordinately with translation errors for key features of myotonic dystrophy pathology to fully manifest.

Author Contributions

SR, JLV, KEP, LC and JC conceived and designed the experiments; SR, JC, KEP, MD, WD, CY, SS, DMD, DBB, JLV, LC performed experiments and analyzed the data; SR, JLV, MD, KEP and JC wrote the manuscript; SR, JC, DMD, KEP, MD, WD, CY, SS DMD, DBB, LC, and JLV discussed and reviewed the manuscript.

Conflict of Interest

Conflicts of interest: none.

Acknowledgments

We thank Dr. Jennifer Darnell for valuable comments, Dr. Maurice Swanson for the *Mbnl1*$^{\Delta E3/\Delta E3}$ mice, Matthew Bancone for assistance with muscle fiber CSA assessment and Dr. Glenn Morris, Dr. Ian Holt and the Muscular Dystrophy Association Monoclonal Antibody Resource (http://www.glennmorris.org.uk/mabs.htm) for the MB2a monoclonal antibodies. Research reported in this publication was supported by NIH/NINDS award number NS060839 (SR) and NIH/NIAMS award numbers AR047664, AR54816, and AR041802 (JLV). The content is solely the responsibility of the authors and does not necessarily represent the official views of the National Institutes of Health.

Appendix A. Supplementary Data

Supplementary data to this article can be found online at http://dx.doi.org/10.1016/j.ebiom.2015.07.028.

References

Adereth, Y., Dammai, V., Kose, N., Li, R., Hsu, T., 2005. RNA-dependent integrin alpha3 protein localization regulated by the muscleblind-like protein MLP1. Nat. Cell Biol. 7, 1240–1247.

Akerman, M., David-Eden, H., Pinter, R.Y., Mandel-Gutfreund, Y., 2009. A computational approach for genome-wide mapping of splicing factor binding sites. Genome Biol. 10, R30.

Batra, R., Charizanis, K., Manchanda, M., Mohan, A., Li, M., Finn, D.J., Goodwin, M., Zhang, C., Sobczak, K., Thornton, C.A., et al., 2014. Loss of MBNL leads to disruption of developmentally regulated alternative polyadenylation in RNA-mediated disease. Mol. Cell 56, 1–12.

Beckmann, R.P., Mizzen, L.E., Welch, W.J., 1990. Interaction of Hsp 70 with newly synthesized proteins: implications for protein folding and assembly. Science 248, 850–854.

Brook, J.D., McCurrach, M.E., Harley, H.G., Buckler, A.J., Church, D., Aburatani, H., Hunter, K., Stanton, V.P., Thirion, J.P., Hudson, T., et al., 1992. Molecular basis of myotonic dystrophy: expansion of a trinucleotide (CTG) repeat at the 3′ end of a transcript encoding a protein kinase family member. Cell 68, 799–808.

Charizanis, K., Lee, K.Y., Batra, R., Goodwin, M., Zhang, C., Yuan, Y., Shiue, L., Cline, M., Scotti, M.M., Xia, G., et al., 2012. Muscleblind-like 2-mediated alternative splicing in the developing brain and dysregulation in myotonic dystrophy. Neuron 75, 437–450.

Dansithong, W., Paul, S., Comai, L., Reddy, S., 2005. MBNL1 is the primary determinant of focus formation and aberrant insulin receptor splicing in DM1. J. Biol. Chem. 280, 5773–5780.

Darnell, J.C., Van Driesche, S.J., Zhang, C., Hung, K.Y., Mele, A., Fraser, C.E., Stone, E.F., Chen, C., Fak, J.J., Chi, S.W., et al., 2011. FMRP stalls ribosomal translocation on mRNAs linked to synaptic function and autism. Cell 146, 247–261.

DiFranco, M., Herrera, A., Vergara, J.L., 2011. Chloride currents from the transverse tubular system in adult mammalian skeletal muscle fibers. J. Gen. Physiol. 137, 21–41.

DiFranco, M., Yu, C., Quinonez, M., Vergara, J.L., 2013. Age-dependent chloride channel expression in skeletal muscle fibres of normal and HSA(LR) myotonic mice. J. Physiol. 591, 1347–1371.

Fardaei, M., Rogers, M.T., Thorpe, H.M., Larkin, K., Hamshere, M.G., Harper, P.S., Brook, J.D., 2002. Three proteins, MBNL, MBLL and MBXL, co-localize in vivo with nuclear foci of expanded-repeat transcripts in DM1 and DM2 cells. Hum. Mol. Genet. 11, 805–814.

Furman, R.E., Barchi, R.L., 1978. The pathophysiology of myotonia produced by aromatic carboxylic acids. Ann. Neurol. 4, 357–365.

Harper, P.S., 2009. Myotonic Dystrophy. second edition. Harcourt Brace Jovanovich Ltd.

Ho, T.H., Charlet-B, N., Poulos, M.G., Singh, G., Swanson, M.S., Cooper, T.A., 2004. Muscleblind proteins regulate alternative splicing. EMBO J. 23, 3103–3112.

Holt, I., Jacquemin, V., Fardaei, M., Sewry, C.A., Butler-Browne, G.S., Furling, D., Brook, J.D., Morris, G.E., 2009. Muscleblind-like proteins: similarities and differences in normal and myotonic dystrophy muscle. Am. J. Pathol. 174, 216–227.

Jaffe, R., Mock, M., Abramowicz, J., Ben-Aderet, N., 1986. Myotonic dystrophy and pregnancy: a review. Obstet. Gynecol. Surv. 41, 272–278.

Jeftinija, D.M., Wang, Q.B., Hebert, S.L., Norris, C.M., Yan, Z., Rich, M.M., Kraner, S.D., 2007. The Ca(V) 1.2 Ca(2+) channel is expressed in sarcolemma of type I and IIa myofibers of adult skeletal muscle. Muscle Nerve 36, 482–490.

Kanadia, R.N., Johnstone, K.A., Mankodi, A., Lungu, C., Thornton, C.A., Esson, D., Timmers, A.M., Hauswirth, W.W., Swanson, M.S., 2003. A muscleblind knockout model for myotonic dystrophy. Science 302, 1978–1980.

Lee, K.Y., Li, M., Manchanda, M., Batra, R., Charizanis, K., Mohan, A., Warren, S.A., Chamberlain, C.M., Finn, D., Hong, H., et al., 2013. Compound loss of muscleblind-like function in myotonic dystrophy. EMBO Mol. Med. 5, 1887–1900.

Lin, X., Miller, J.W., Mankodi, A., Kanadia, R.N., Yuan, Y., Moxley, R.T., Swanson, M.S., Thornton, C.A., 2006. Failure of MBNL1-dependent post-natal splicing transitions in myotonic dystrophy. Hum. Mol. Genet. 15, 2087–2097.

Lueck, J.D., Mankodi, A., Swanson, M.S., Thornton, C.A., Dirksen, R.T., 2007. Muscle chloride channel dysfunction in two mouse models of myotonic dystrophy. J. Gen. Physiol. 129, 79–94.

Mankodi, A., Takahashi, M.P., Jiang, H., Beck, C.L., Bowers, W.J., Moxley, R.T., Cannon, S.C., Thornton, C.A., 2002. Expanded CUG repeats trigger aberrant splicing of ClC-1 chloride channel pre-mRNA and hyperexcitability of skeletal muscle in myotonic dystrophy. Mol. Cell 10, 35–44.

Nelson, R.J., Ziegelhoffer, T., Nicolet, C., Werner-Washburne, M., Craig, E.A., 1992. The translation machinery and 70 kd heat shock protein cooperate in protein synthesis. Cell 71, 97–105.

Onishi, H., Kino, Y., Morita, T., Futai, E., Sasagawa, N., Ishiura, S., 2008. MBNL1 associates with YB-1 in cytoplasmic stress granules. J. Neurosci. Res. 86, 1994–2002.

Paul, S., Dansithong, W., Kim, D., Rossi, J., Webster, N.J., Comai, L., Reddy, S., 2006. Interaction of muscleblind, CUG-BP1 and hnRNP H proteins in DM1-associated aberrant IR splicing. EMBO J. 25, 4271–4283.

Paul, S., Dansithong, W., Jog, S.P., Holt, I., Mittal, S., Brook, J.D., Morris, G.E., Comai, L., Reddy, S., 2011. Expanded CUG repeats dysregulate RNA splicing by altering the stoichiometry of the muscleblind 1 complex. J. Biol. Chem. 286, 38427–38438.

Paz, I., Akerman, M., Dror, I., Kosti, I., Mandel-Gutfreund, Y., 2010. SFmap: a web server for motif analysis and prediction of splicing factor binding sites. Nucleic Acids Res. 38, W281–W285.

Personius, K.E., Arbas, E.A., 1998. Muscle degeneration following remote nerve injury. J. Neurobiol. 36, 497–508.

Personius, K.E., Sawyer, R.P., 2006. Variability and failure of neurotransmission in the diaphragm of mdx mice. Neuromuscul. Disord. 16, 168–177.

Poulos, M.G., Batra, R., Li, M., Yuan, Y., Zhang, C., Darnell, R.B., Swanson, M.S., 2013. Progressive impairment of muscle regeneration in muscleblind-like 3 isoform knockout mice. Hum. Mol. Genet. 22, 3547–3558.

Ranum, L.P.W., Cooper, T.A., 2006. RNA-mediated neuromuscular disorders. RNA. Annu. Rev. Neurosci. 29, 259–277.

Reddy, S., Smith, D.B., Rich, M.M., Leferovich, J.M., Reilly, P., Davis, B.M., Tran, K., Rayburn, H., Bronson, R., Cros, D., et al., 1996. Mice lacking the myotonic dystrophy protein kinase develop a late onset progressive myopathy. Nat. Genet. 13, 325–335.

Wang, E.T., Cody, N.A., Jog, S., Biancolella, M., Wang, T.T., Treacy, D.J., Luo, S., Schroth, G.P., Housman, D.E., Reddy, S., et al., 2012. Transcriptome-wide regulation of pre-mRNA splicing and mRNA localization by muscleblind proteins. Cell 150, 710–724.